Applied Geochemistry 203 (2026) 106812

Contents lists available at ScienceDirect

Applied Geochemistry

journal homepage: www.elsevier.com/locate/apgeochem

Evaluation of rock resources for carbon dioxide removal by enhanced weathering: A South China case

Shan Qi, Xing Jian *

State Key Laboratory of Marine Environmental Science, College of Ocean and Earth Sciences, Xiamen University, Xiamen, 361102, PR China

ARTICLE INFO

Handling Editor: G. Bird

Keywords:
Enhanced rock weathering
Carbon dioxide removal
Geochemistry data-analysis
Ultra-mafic and mafic rock
Weathering carbon sink

ABSTRACT

With the challenge of rising atmospheric CO_2, Enhanced Rock Weathering (ERW) has emerged as a promising climate mitigation strategy. By spreading ground weatherable rocks (mostly mafic and ultra-mafic silicate rocks) to cropland, forest and coast in climatically favorable regions, ERW is thought to involve both benefits and environmental risks. While previous studies have mainly focused on carbon removal abilities and efficiencies of the most favorable minerals and rocks, high-potential rock resource surveys and comprehensive regional assessments integrating diverse beneficial and risk factors are poorly reported. In this contribution, we bridged this gap by first establishing a robust geochemical database of 7037 mafic and ultramafic rock samples across South China. Using this database, we developed a multi-criteria evaluation framework considering weathering potential, nutrients, heavy metals, and local climatic factors. The weight allocation in the system was determined by the Inter-criteria Correlation (CRITIC) method and subjective adjustment to assess the ERW potential of these rocks. The evaluation results reveal significant potential in Fujian Province, which we identify as the optimal location, with Guangdong, Jiangxi, and Hainan provinces being highly suitable alternatives. The coastlines of Guangdong, Hainan and southwestern Guangxi provinces are also ideal sites for coastal ERW deployment. Furthermore, high-potential rocks are often characterized by metamorphism and high iron oxide content, such as metamorphosed harzburgite from the Fujian coast, gabbro from the Emeishan Large Igneous Province (ELIP) in southwestern China, and pyroxenite from Henan Province. These findings offer actionable insights for policymakers and developers, enabling targeted resource allocation and accelerating ERW adoption. While heavy metal elements like copper, cadmium, and lead require careful environmental monitoring, the study provides a practical roadmap for ERW deployment. Our multi-criteria assessment framework serves as a standardized approach for a local or regional ERW resource assessment that can contribute to global CO_2 removal strategies. Future work should refine this methodology by incorporating mineralogical compositions for greater precision and validating findings through in-situ field trials to assess real-world CO_2 removal rates and heavy metal bioavailability. The comprehensive database established here provides a foundational resource for these future endeavors and other geological applications.

1. Introduction

Both observation (Keeling et al., 2001; Monnin et al., 2001) and modeling (IPCC, 2021) results strongly support the continuous rising of atmospheric CO_2 concentrations since the Industrial Revolution, reaching 286 ppm in 1860 (Etheridge et al., 1996), about 369 ppm in 2000, and 426 ppm in March 2025 (Lan et al., 2025). Increasing CO_2 concentrations may cause various hazards like global warming, extreme climatic events, rising sea level, etc., which might seriously threaten humanity (Bazzaz, 1990; Van Groenigen et al., 2011; Shakun et al., 2012; Gao et al., 2012). To mitigate this concerning situation, 195 countries agreed to curb anthropogenic CO_2 emissions to limit warming to 1.5 °C above preindustrial levels at the 2015 UN Climate Change Conference in Paris. However, despite rising awareness of the need to reduce emissions, atmospheric CO_2 levels continue to rise, necessitating additional strategies for carbon mitigation (UNFCCC, 2015; Horowitz, 2016; Baker et al., 2018). Under such circumstances, Carbon Dioxide Removal (CDR), involving several methods and techniques (Terlouw et al., 2021; Fuhrman et al., 2023), has been proposed and expected to play a crucial role in all 1.5 °C scenarios necessary to meet related goals

* Corresponding author.
E-mail address: xjian@xmu.edu.cn (X. Jian).

https://doi.org/10.1016/j.apgeochem.2026.106812
Received 11 August 2025; Received in revised form 22 March 2026; Accepted 1 April 2026
Available online 3 April 2026

(Smith et al., 2024).

Enhanced Rock Weathering (ERW) is emerging as one of the promising CDR approaches (Schuiling and Krijgsman, 2006; Hartmann et al., 2013; Beerling et al., 2018). The main realization route of ERW is sequestering CO_2 by applying ground weatherable rocks (mostly silicate rocks) to cropland, forest and coastal regions (Fig. 1). The great potential of ERW in CDR solutions originates from the rationale that continental weathering, particularly silicate rock chemical weathering, plays a crucial role in carbon cycles and in regulating global climate (Penman et al., 2020). Specifically, chemically reactive minerals in silicate rocks such as feldspar, pyroxene and olivine, could consume CO_2 during chemical weathering in water-rich environments, generating alkalinity and dissolved inorganic carbon that can be transported to aquatic systems or incorporated into carbonate phases over time. This process generates magnesium, calcium and bicarbonate ions that remain dissolved, preventing their conversion into atmospheric CO_2 through equilibrium, increasing alkalinity in soil waters and leachates (Hartmann et al., 2013; Larkin et al., 2022; Vienne et al., 2022). A substantial fraction of this alkalinity can be transported through catchments to rivers and then oceans, where it represents long-term CO_2 storage as ocean dissolved inorganic carbon (DIC) and ultimately marine carbonates (Schuiling and Krijgsman, 2006; Bertagni and Porporato, 2022; Haque et al., 2020). Serving as another pathway, at sufficiently high pH, dissolved ions and DIC can precipitate as secondary (pedogenic) carbonates in soils and subsoils, storing CO_2 as solid inorganic carbon (Vienne et al., 2022; Khalidy et al., 2023; Cong et al., 2024). Modern atmospheric CO_2 drawdown through weathering of silicate rocks, as one of the major carbon sinks, has been well qualitatively and quantitatively described in many previous studies (e.g., Kasting and Catling, 2003; Dessert et al., 2003; Lee et al., 2019). Throughout the geological history, several global cooling events were also attributed to this CO_2 drawdown effect through large-scale silicate (especially mafic and ultra-mafic) weathering processes (Goddéris et al., 2017; Conwell et al., 2022; Bayon et al., 2023; Murray and Jagoutz, 2024).

It has been evaluated that the natural weathering of silicate and calcium carbonate rocks sequesters approximately 0.25 Pg C annually, which is only 3% of the yearly emission of oil burning (Taylor et al., 2016). Thus, natural weathering rates are insufficient for the goal of carbon neutrality. Accelerating this process through ERW could significantly enhance its natural capacity, offering a viable solution to mitigate anthropogenic emissions (Schuiling and Krijgsman, 2006; Renforth, 2012; Renforth et al., 2015; Taylor et al., 2016; Beerling et al., 2018). Furthermore, ERW can also ameliorate ocean acidification, release elements from minerals such as K, Si and P to help stimulate biological production (Goll et al., 2021; Riebesell et al., 2007), increase lithosphere carbon sink and boost biological pump in the ocean to settle carbon (Hartmann et al., 2013). However, large-scale implementation of ERW may also entail environmental risks, most notably the potential mobilization of trace heavy metals from mineral feedstocks into soil and aquatic ecosystems (Haque et al., 2020; Flipkens et al., 2021; Dupla et al., 2023). In recent years, the ERW potential has been tested mainly over models (Beerling et al., 2020; Fuhrman et al., 2023) and field experiments (Buckingham et al., 2022; Beerling et al., 2024; Holden et al., 2024; Linke et al., 2024). Projections suggest that ERW could sequester 0.5 to 2 gigatonnes of CO_2 annually in China alone, with costs ranging from US $ 80 to 180 per tonne of CO_2 removed (Beerling et al., 2020; Guo et al., 2023). This promises the future for higher contributions to reaching global CDR goals (Eufrasio et al., 2022). In addition, ERW is expected to require less water, energy and costs than other CDR methods (Eufrasio et al., 2022; Kantzas et al., 2022). Optimizing rock selection and application areas may further enhance cost efficiency and overall effectiveness. To quantify sequestration potential and risks, a systematic rock resource survey is necessary to understand the mineral composition and elemental content of silicate rocks and to understand the potential of resource utilization for ERW (Guo et al., 2023).

In this contribution, we took South China as a case and targeted on ultra-mafic, mafic and a minor portion of intermediate rocks for their potentially high carbon dioxide sequestration efficiency. South China is selected as our investigated area mainly because of its humid and warm climate advantages which are critical factors controlling weathering processes. We collected mineralogical, petrographic, geochemical and age data from previous geological case studies (involving 7037 rock samples from 377 literatures (from 1980 to 2024), see Tables S1 and S2) across South China. A rock resource database was set up and ERW evaluation frameworks were established for different possible implementation situations. There are several important parameters considered in our evaluation frameworks including rock qualities, climate background, study intensity, heavy metals, nutrients released by rock application and transportation distances. Different application areas and environmental demands are also considered. The aims of this study are 1) to create a comprehensive dataset for mafic and ultra-mafic rocks across South China; 2) to provide evaluation methods and results for ERW rock utilization and deployment areas; 3) to better understand ERW application and to contribute to global carbon removal efforts.

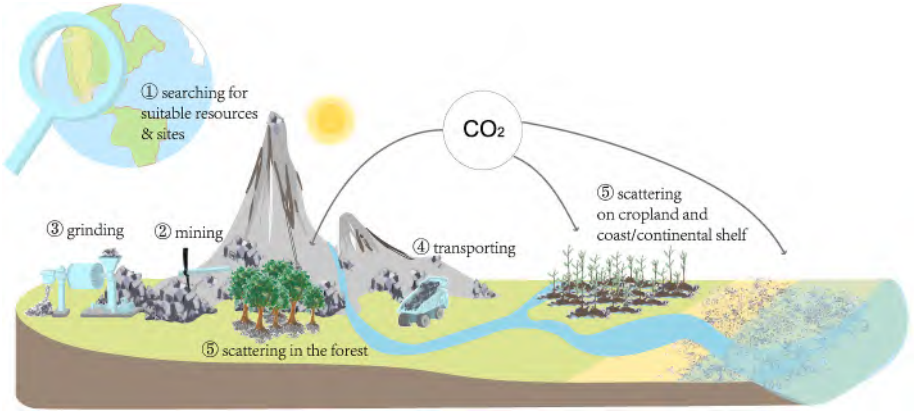

Fig. 1. Conceptual Framework of Enhanced Rock Weathering (ERW) Processes. Major procedure includes: ①searching for suitable rock resources and sites,②mining for the rock, ③grinding rock into particles (preferably 1 mm diameter, Moosdorf et al., 2014), ④transporting the particles to the field, ⑤scattering the rock pieces in forests, or on croplands/beaches/continental shelves and monitoring total Carbon Dioxide Removal (CDR) and environmental consequences. Following silicate weathering sequesters CO_2 and stores it in the ocean as inorganic carbon (e.g., HCO_3^-, $CaCO_3$) for 10 to 100 million years (Renforth and Henderson, 2017). Searching for suitable rock resources is a crucial step for ERW and the theme of this study.

2. Background

2.1. Enhanced rock weathering for atmospheric carbon dioxide removal

As proposed in previous studies (Spence et al., 2021; Cong et al., 2024), the procedure of ERW implementation contains five basic stages (Fig. 1). Numerous studies through theoretical calculation and simulation have drawn attention to the rock grinding process, since it is thought to be the most energy-consuming process in ERW implementation (Moosdorf et al., 2014; Beerling et al., 2018). While minimum crushing energy occurs at millimetre scale (~1 mm, Moosdorf et al., 2014), significant net CO_2 drawdown may require much finer particles (<45–10 μm, Rinder and Hagke, 2021; Vanderkloot and Ryan, 2023). Additionally, other procedures might generate secondary CO_2 emissions, especially for the transportation process. Using functions between cropland areas and the global transportation system, the optimum transporting distance between material resources and application areas in warm regions was calculated as less than 300 km (Strefler et al., 2018). When silicate rock grains are applied to forests or croplands, carbon removal occurs via two main pathways: alkalinity export and potential secondary carbonate precipitation (Haque et al., 2020; Larkin et al., 2022; Vienne et al., 2022; Sokol et al., 2024). Terrestrial ERW is therefore tightly coupled with complex biogeochemistry. Weathering rates are accelerated by high soil pCO_2 from roots and microbes (Deng et al., 2023), but net efficiency depends heavily on hydrology and soil properties (Lan et al., 2025). In contrast, coastal ERW (on the coast and continental shelf) bypasses this terrestrial complexity by exposing minerals directly to well-mixed seawater. This acts as direct ocean alkalinity enhancement, benefiting from rapid dilution in a stable alkaline reservoir (Hartmann et al., 2013; Foteinis et al., 2023). The effect of ERW has also been widely examined through several pilot field tests, such as the Illinois field trials (Blanc-Betes et al., 2021; Kantola et al., 2023; Beerling et al., 2024); a series of tests in several locations (e.g., Yolo, Merced) across California (Sokol et al., 2024). These pilot field tests mainly focused on quantifying the accumulated CO_2 sequestration and discovering co-benefits (e.g., enhanced crop yield, reduced N_2O emissions; Skov et al., 2024). While irrigated cropland field trials (Sokol et al., 2024) primarily focused on organic carbon dynamics, they also reported potential carbonate mineral precipitation in the upper soil. Similarly, soil pore water samples from California (Holzer et al., 2023) demonstrated carbonic acid weathering via elevated bicarbonate concentrations in the upper soil (0–30 cm), though the subsequent export and permanent sequestration of this carbon remain to be fully quantified. Although ERW has been raised for a couple of years, it is still in the primary stage of development and needs multi-disciplinary argumentative analysis and intellectual input in the fields of geochemistry, ecology, soil science, environmental science, economics, and social sciences, etc.

From a geoscience perspective, the rock resource searching and planning procedure before mining needs to be considered. However, this has been nearly neglected in current ERW evaluations. Peridotite consisting of pure forsterite exhibits a maximum CO_2 sequestration of 1.25 t CO_2 per ton of rock (Moosdorf et al., 2014), though the effect of basalts is proposed to be approximately 0.3 t CO_2 per ton of rock (Renforth, 2012). Nevertheless, studies show that ultramafic rocks (e.g., peridotite) typically harbor much higher levels of trace metals, such as Ni and Cr, than mafic rocks like basalt (Beerling et al., 2018). These elements can be released into the surrounding environment through mineral dissolution, potentially leading to soil contamination or water toxicity. Therefore, it is crucially important to search for the best rock sources before implementing.

2.2. Weathering advantages of mafic and ultra-mafic silicate rocks

Silicate rock is widespread on the Earth's surface, but it has a rather low weathering rate. Calcium carbonate rocks have a higher weathering rate but less advantage for increasing carbon sink, as their weathering on acidic soil eventually leads to the CO_2 they contain being released into the solution and degassed to the atmosphere (Hamilton et al., 2007). Pure calcium carbonate minerals contain little or no silicon and provide few of the essential nutrients required by plants and crops. Although natural carbonate rocks often include minor silica in the form of quartz, clay minerals, or chert, their overall nutrient content remains low (Beerling et al., 2018). From an efficiency perspective, mafic and ultra-mafic silicate rocks are the most suitable rock type for implementing ERW, because they are composed of abundant chemically reactive minerals.

To optimize the weathering rate during silicate rock application for ERW, it is crucial to consider the dissolution kinetics of different minerals (Hartmann et al., 2013). At a neutral pH of 7, dissolution rates (in mol mineral $m^{-2}s^{-1}$) vary significantly: for instance, larnite exhibits a high rate of approximately 10^{-6}, followed by fayalite (10^{-9}), forsterite (10^{-10}), anorthite (10^{-11}), and diopside (10^{-11}), while hornblende and glaucophane show slower rates around 10^{-12} and 10^{-11} (Table 1). For bulk rock, the dissolution rate of basalt is approximately 2×10^{-11} mol mineral $m^{-2}s^{-1}$ at pH = 7 (Brantley, 2008). This rate would increase with enhanced soil alkalinity, a direct outcome of ERW application (Brantley, 2008). Building on previous research that focused predominantly on peridotite and basalt (Renforth and Henderson, 2017; Beerling et al., 2020; Hakim et al., 2021; Kantzas et al., 2022; Ali et al., 2025), our study expands this scope by emphasizing the broader range of ultramafic and mafic rock types.

2.3. Environmental consequences for ERW

Although ultra-mafic rocks are considered to have higher weathering efficiency than mafic rocks, most ultra-mafic materials are relatively enriched in several heavy elements (e.g., Cr, Ni and Co in the crystal structure of olivine and pyroxene; Kierczak et al., 2021). Inevitably, the spread of ultra-mafic rocks would herald great environmental contamination and possible harm to human health. In most ERW plans involving the application of ground rocks in croplands, large-scale spreading of such rocks may interfere with plant physiological processes and internal antioxidant systems, potentially reducing crop yields and introducing harmful heavy metals into the food chain (Ramos et al., 2022). However, the specific harmful heavy metals are not clearly defined. There are differing opinions. For example, most studies identify Cr and Ni as key heavy metals (Haque et al., 2020). Some researchers suggest that Ni is considerably low in peridotite, which will not affect cropland if spread, and Cr mostly appears to be insoluble particles that are inaccessible to organisms (Schuiling and Krijgsman, 2006). Instead, continental flood basalt has a relatively low concentration of heavy metals, thus it is less adverse for the environment. Mafic dikes also have multiple elements that have benefits for crop growing, such as phosphorus (P), potassium (K), calcium (Ca), magnesium (Mg), and iron (Fe) (Beerling et al., 2018). Some elements in rock powder may be seen as fertilizer and prompt the growth of various plants, including crops and trees. It is suggested that basalt releases base cations at relatively moderate rates, contributing to gradual soil alkalinization. However, the effectiveness of this process may be influenced by SiO_2 polymerization, sorption of released cations, and the formation of secondary minerals (Buckingham et al., 2022). These processes may reduce the availability of base cations to charge-balance bicarbonate, thereby delaying or limiting the export of alkalinity and associated CO_2 removal, while in some cases secondary mineral formation may also influence weathering kinetics by modifying saturation states.

In South China, where many agricultural and forest soils are strongly acidic (commonly pH 4.5–5.5, Guo et al., 2018; Sun et al., 2020; Han et al., 2022), ERW-induced alkalinization may provide agronomic and ecological co-benefits by alleviating acid stress, reducing Al and Fe toxicity, and moving soil pH toward the generally optimal range of approximately 5.5–6.5 for most crops and soil microbial communities

Table 1
Weathering reaction and dissolution rate for fast-weathered silicate minerals.

Mineral		Chemical reaction	Dissolution rate at pH 7, 25 °C (mol mineral $m^{-2}s^{-1}$)	Dissolution rate at pH 6, 25 °C (mol mineral $m^{-2}s^{-1}$)	Dissolution rate at pH 5, 25 °C (mol mineral $m^{-2}s^{-1}$)
Olivine minerals	Fayalite	$2Fe_2SiO_4 + 8CO_2 + 8H_2O + O_2 \rightarrow 4Fe^{3+} + 8HCO_3^- + 2H_4SiO_4 + 2H_2O \rightarrow$ Goethite (FeOOH) or other Fe-oxides $+ 8HCO_3^- + 2H_4SiO_4$	$10^{-8.60}$	$10^{-8.32}$	$10^{-8.02}$
	Forsterite	$Mg_2SiO_4 + 4CO_2 + 4H_2O \rightarrow 2Mg^{2+} + 4HCO_3^- + H_4SiO_4$	$10^{-9.53}$	$10^{-9.24}$	$10^{-8.94}$
Pyroxene minerals	Diopside	$CaMgSi_2O_6 + 2H_2CO_3 + 2H_2O \rightarrow CaCO_3 + MgCO_3 + 2H_4SiO_4$	$10^{-11.00}$	$10^{-10.95}$	$10^{-10.86}$
Feldspar minerals	Anorthite	$CaAl_2Si_2O_8 + H_2CO_3 + H_2O \rightarrow CaCO_3 + Al_2Si_2O_5(OH)_4$	$10^{-11.11}$	$10^{-11.18}$	$10^{-10.92}$
	Bytownite	$(Ca_{0.7}Na_{0.3})Al_{1.7}Si_{2.3}O_8 + 3.7CO_2 + 4H_2O \rightarrow 0.7Ca^{2+} + 0.3Na^+ + 1.7Al^{3+} + 3.7HCO_3^- + 2.3H_4SiO_4$	$10^{-11.06}$	$10^{-11.14}$	$10^{-10.99}$
	Labradorite	$(Ca_{0.7}Na_{0.3})Al_{1.7}Si_{2.3}O_8 + 3.7CO_2 + 4H_2O \rightarrow 0.7Ca^{2+} + 0.3Na^+ + 1.7Al^{3+} + 3.7HCO_3^- + 2.3H_4SiO_4$	$10^{-11.07}$	$10^{-11.14}$	$10^{-10.99}$
Amphibole minerals	Hornblende	$Ca_2Mg_5Si_8O_{22}(OH)_2 + 10CO_2 + 12H_2O \rightarrow 2Ca^{2+} + 5Mg^{2+} + 10HCO_3^- + 8H_4SiO_4$	$10^{-12.12}$	$10^{-12.06}$	$10^{-11.95}$
	Glaucophane	$Na_2Mg_3Al_2Si_8O_{22}(OH)_2 + 12CO_2 + 12H_2O \rightarrow 2Na^+ + 3Mg^{2+} + 2Al^{3+} + 12HCO_3^- + 8H_4SiO_4$	$10^{-11.17}$	$10^{-10.59}$	$10^{-9.91}$
Other minerals	Larnite	$Ca_2SiO_4 + 2CO_2 + 2H_2O \rightarrow 2Ca^{2+} + 2HCO_3^- + H_4SiO_4$	$10^{-5.96}$	$10^{-5.68}$	$10^{-5.38}$
	Wollastonite	$CaSiO_3 + 2CO_2 + 3H_2O \rightarrow Ca^{2+} + 2HCO_3^- + H_4SiO_4$	$10^{-8.67}$	$10^{-8.49.}$	$10^{-8.31}$

Note: specific testing and equations of dissolution rates for each mineral were mentioned in Heřmanská et al. (2022). For wollastonite, it is cited from Schott et al. (2012).

(Yang et al., 2022; Xiong et al., 2024). However, excessive pH increases beyond crop-specific optima could negatively affect plant performance, indicating that ERW application rates should be carefully managed according to soil type and cropping system. In addition, ERW may alter soil carbon cycling beyond inorganic carbon formation. Increases in soil pH can accelerate organic matter decomposition, while contrasting and still poorly quantified responses of particulate and mineral-associated organic carbon pools have been reported (Sokol et al., 2024). Given that modelling studies project the largest human health impacts of ERW in countries such as China (Eufrasio et al., 2022), our evaluation framework explicitly considers both nutrient supply and potentially toxic elements, acknowledging that the risks and benefits associated with heavy-metal release remain an active area of debate and require site-specific assessment.

2.4. Geological and climatic background of South China

We select the southern part of China, rather than North China, to conduct rock resource evaluation for ERW mainly because of its climate benefits (Fig. 2a; Fig. 2b; Fig. 2c; Fig. S1). Koppen's climate classification reveals that South China dominantly has Cf (Subtropical humid climate) and Cw (Subtropical dry-winter) climate types (Fig. 2a). For these climate types, there must be 8–12 months with monthly average temperature higher than 10 °C, and monthly precipitation above certain value (Belda et al., 2014), indicating humid and warm for most time of the year, favoring intense chemical weathering. The warmth and moisture are provided by the East Asian Summer Monsoon, whose intensity and variability will continue to grow under the global warming 2 °C scenario according to modelling results (You et al., 2022; Xue et al., 2023). The moist climate in South China is no doubt beneficial to the application of ERW since weathering rates decline sharply at dryness index $D_r > 1$ (Calabrese et al., 2022). As mentioned above, the rock material transporting distance would affect ERW efficiency and costs (<300 km in warm regions best, Strefler et al., 2018). Accordingly, even if there are plenty of ultra-mafic and mafic rocks in North China (Hartmann and Moosdorf, 2012), which is characterized by its dry climate, it is not appropriate to transport rocks to South China for implementing ERW. Therefore, rocks in North China are excluded from our evaluation.

The land use in South China contains various kinds, including forest, cropland, wetland, etc. Based on the main data of the Third National Land Survey released by the Ministry of Natural Resources, the gross cropland and forest areas in southern China have reached over 2,100,000 km^2 (Fig. 2d). The vegetation is mostly composed of broad-leaved evergreen/warm mixed forest, a portion of tropical rainy forest and tropical seasonal forest in the southern part of Hainan Province (Wu et al., 2021), which provides a broad land area for ERW application. The topography of South China is characterized by high elevations in the west, gradually flattening towards the east, allowing rivers to transport the inorganic carbon from field to ocean (Fig. 2e). The rivers and drainage networks in South China cover almost the entire potential ERW application areas (Fig. 2f), providing both opportunities for direct application to streams and efficient transport pathways for weathering products (e.g. HCO_3^-, Mg^{2+}, Ca^{2+}) from soils to rivers (Hill and Peart, 1998). Furthermore, the extensive coastal margin, particularly its western and southern stretches, offers diverse environments suitable for both types of coastal ERW application (Meysman and Montserrat, 2017). Strong wave dynamics along the southeast coast and within bays provide ideal conditions for "shelf milling", while abundant coastal biota would further enhance the dissolution process.

There are several cities, provinces and areas in South China that we did not consider in this study, as they are highly urbanized hence lack croplands for ERW applications. For example, Shanghai, Hong Kong, Macao and several islands within the South China Sea (SCS) area are not considered due to a lack of data and the relatively small application area. Taiwan is excluded for its surface rock resources are mostly sedimentary rocks and slightly metamorphosed rocks (Zhang et al., 2022). The city of Chongqing is actually not considered in the evaluation as samples from this region are removed in the data cleaning process (Section 3.2), however the samples are included in the originally compiled (Table S1).

3. Data resources and evaluation methods

3.1. Data collection and descriptions

We collected raw data of mafic and ultra-mafic silicate rocks (7037 rock samples) from 377 published papers (see the supplementary materials). These literatures mainly focus on petrogenesis, tectonic evolution and geochemistry studies. In our compiled dataset, information includes sample name, coordinate location, age, rock type, rock name, major and trace element geochemistry, radiogenic isotopic ratio and mineral composition if there is any.

The dataset covers various kinds of regions, rock types and forming periods (Fig. 3; Fig. S2; Fig. S3; Fig. S4). The Proterozoic ophiolite rocks along the Shaoxing-Pingxiang-Longsheng (spanning Zhejiang, Jiangxi, Hunan, and Guangxi provinces) and Dongxiang-Dexing-Shexian zones

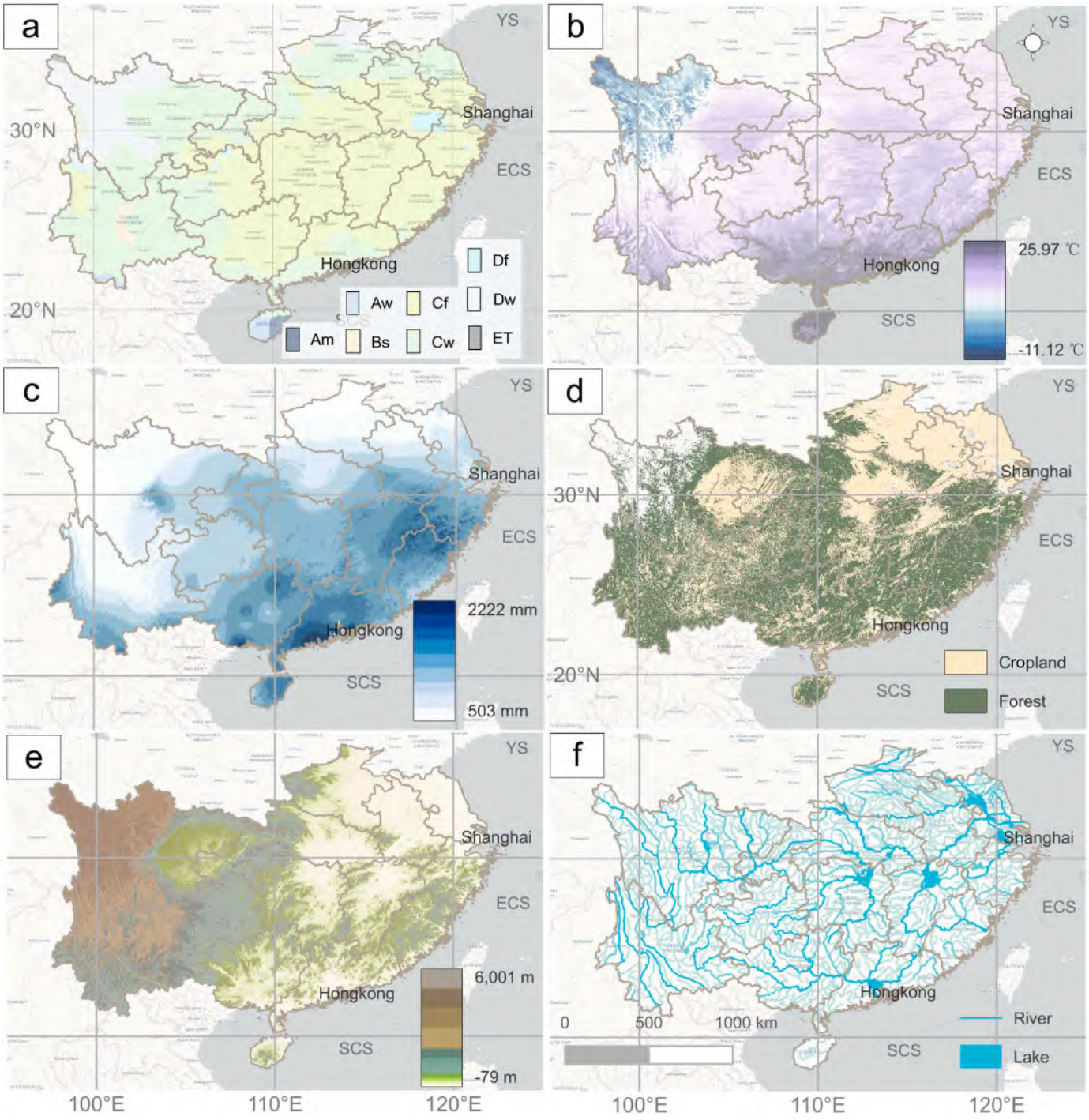

Fig. 2. Environmental factors and geological features relevant to rock weathering in South China. The topography of South China is characterized by high elevations in the west, gradually flattening towards the east. Small plains are present in the northwest, while the southern areas are predominantly hilly. The climate becomes progressively hotter and more humid at lower elevations due to monsoon influences, with southeastern and coastal regions maintaining consistently high average annual temperatures and precipitation. The area boasts extensive forest and cultivated land, with forests occupying a larger proportion due to topographic factors. The hydrological system is dominated by the Yangtze River, a major water source for Southern China, along with its well-developed network of tributaries. YS: Yellow sea; ECS: East China sea; SCS: South China sea. (a) Köppen climate zones (Am: tropical monsoon; Aw: tropical savanna; Bs: semi-arid; Cf: temperate, fully humid; Cw: temperate with dry winter; Df: cold, fully humid; Dw: cold with dry winter; ET: tundra; Beck et al., 2018); (b) Average annual temperature (2012–2022); (c) Average annual precipitation (2012–2022); (d) Land use patterns (Yang and Huang, 2024); (e) Topography (elevation); (f) Hydrological network (rivers). (For interpretation of the references to color in this figure legend, the reader is referred to the Web version of this article.)

(spanning Anhui and Jiangxi provinces) were mainly formed by the Neoproterozoic assembly of the Yangtze and Cathaysia Blocks following the subduction-accretion of the Paleo-South China Ocean and the closure of the Huaiyu back-arc marginal sea (Shu et al., 2021). The flood basalts in Sichuan, Yunnan and Guizhou provinces are called the Emeishan Large Igneous Province (ELIP), formed due to late Permian mantle plume magmatism (Ali et al., 2005; Shellnutt, 2014). Cretaceous mafic and ultra-mafic rocks are mainly distributed in the Cathaysia Block (particularly across Fujian, Zhejiang, Guangdong, and Jiangxi provinces), which are the result of lithospheric extension and thinning

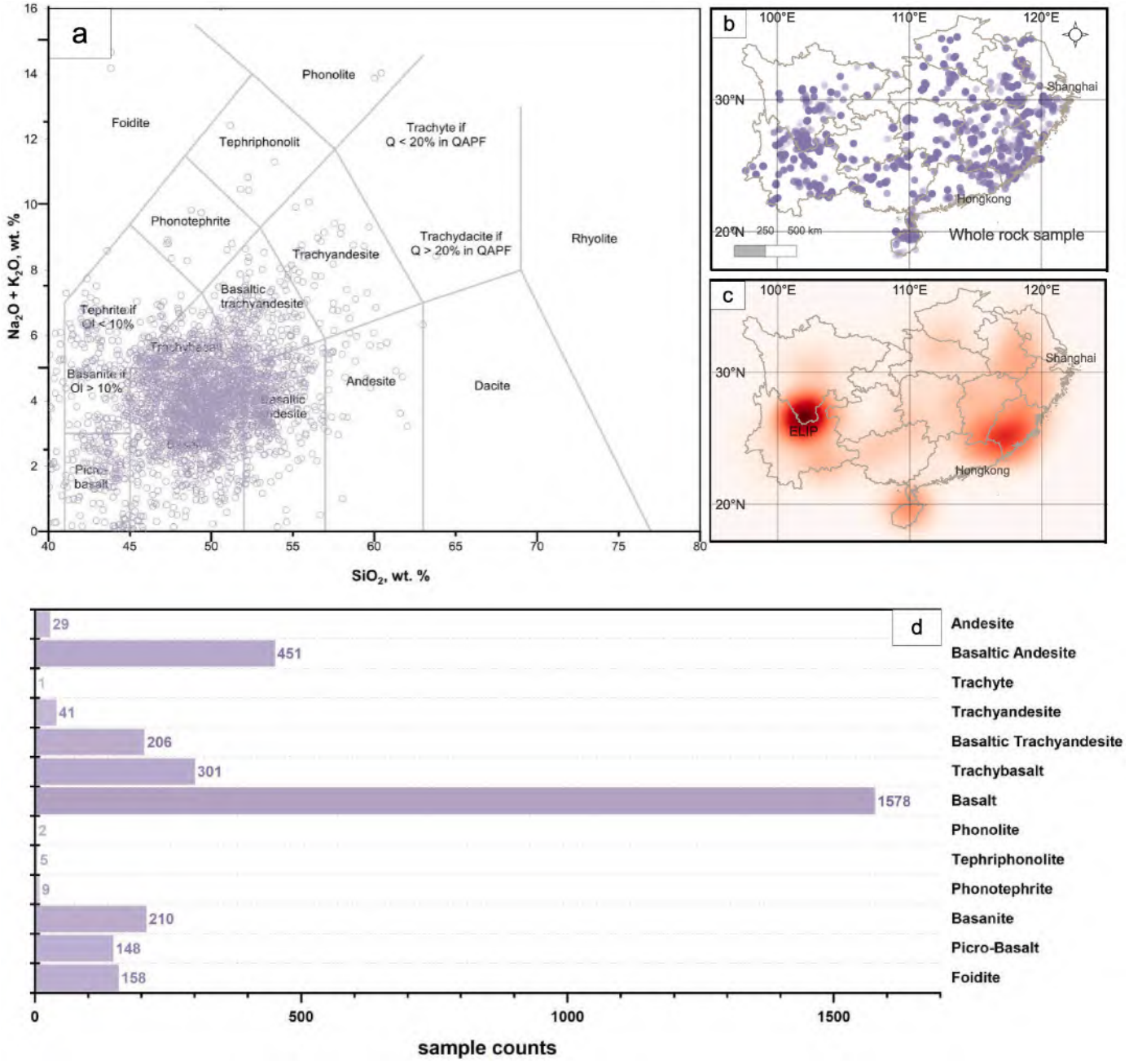

Fig. 3. Characteristics and Spatial Distribution of Sampled Rock Types. (a) Total Alkali-Silica (TAS) Diagram for ultra-mafic and mafic rocks. This diagram classifies the analyzed rock types based on their SiO_2 and $Na_2O + K_2O$ content, illustrating their geochemical relationships. There are only 3139 samples on panel (a) and (d) after filtering, leaving the samples of LoI ≤2% and Total of 98~102%. (b) Spatial distribution of all sampled localities (all samples from the compiled dataset before quality filtering). This map shows the geographical coordinates of each rock sample collected within the study area. (c) Heatmap illustrates the spatial density of sampled rock locations. Higher intensity (warmer colors) indicates a greater concentration of sample points, with notable hotspots observed near coastal lines of Fujian Province and within the Emeishan Large Igneous Province (ELIP). (d) Distribution of rock types by sample count. This bar chart presents the relative abundance of different rock types in the sample set, indicating the number of samples collected for each lithology. (For interpretation of the references to color in this figure legend, the reader is referred to the Web version of this article.)

driven by the Paleo-Pacific Plate's rollback and increasing subduction angles (from low to high angles). This led to the upwelling of asthenospheric mantle and subsequent partial melting of both the enriched subcontinental lithospheric mantle and lower crust (Li et al., 2014, 2015) and thus resulted in diverse magmatic products, including basaltic rocks and associated intrusions. In addition, there are multiple studies focusing on Cenozoic volcanic activities along the southern coast, especially in Fujian and Hainan provinces. These Cenozoic rocks are thought to be linked to the post-subduction processes following the cessation of Paleo-Pacific plate subduction and the subsequent rifting and seafloor spreading of the SCS (Zhou et al., 2006; Chen et al., 2008; He et al., 2020).

3.2. Data validation and organization

The dataset comprises comprehensive major element (e.g., SiO_2, TiO_2, Al_2O_3, TFe_2O_3, MnO, MgO, CaO, Na_2O, K_2O, P_2O_5) and trace element (e.g., Rare Earth Elements (REE), High Field Strength Elements (HFSE), Large-Ion Lithophile Elements (LILE), transition metals, especially emphasis on potentially toxic elements like Cr, Co, Ni, Cu, Zn, Ag,

As, Pb, Cd, Sn, Hg) geochemical analysis results from various rock samples. The geochemical data were primarily derived from X-ray fluorescence (XRF) analyses for major elements, complemented by a range of analytical techniques for trace elements, including atomic absorption spectrometry (AAS), atomic emission spectrometry (AES), instrumental neutron activation analysis (INAA), inductively coupled plasma mass spectrometry (ICP-MS), and routine wet chemistry, as reported in the original sources. For the purpose of ERW rock suitability assessment, particular attention was paid to nutrient elements (Na_2O, K_2O, P_2O_5), weathering indicators, and potentially toxic elements (heavy metals). It is noted that not all the element data were present in each literature, except for SiO_2, presenting a challenge for comprehensive analysis. We realized that the element Fe has several presentation forms. To ensure data consistency, all total iron values, irrespective of their original reported form (Fe_2O_3, FeO, or TFeO), were uniformly converted to total iron expressed as TFe_2O_3 if needed. Harzburgite samples containing serpentinised olivine were excluded from further evaluation due to their altered mineralogical state and associated environmental concerns.

A significant data gap existed due to incomplete GPS coordinates for most samples. To resolve this, we manually geocoded each sample by cross-referencing its descriptive location narrative (including province and other specified local features) with the schematic geological map provided in the literature. This process allowed for the compilation of a complete and spatially accurate coordinate dataset for subsequent analysis. The collected geochemical and GPS data were then

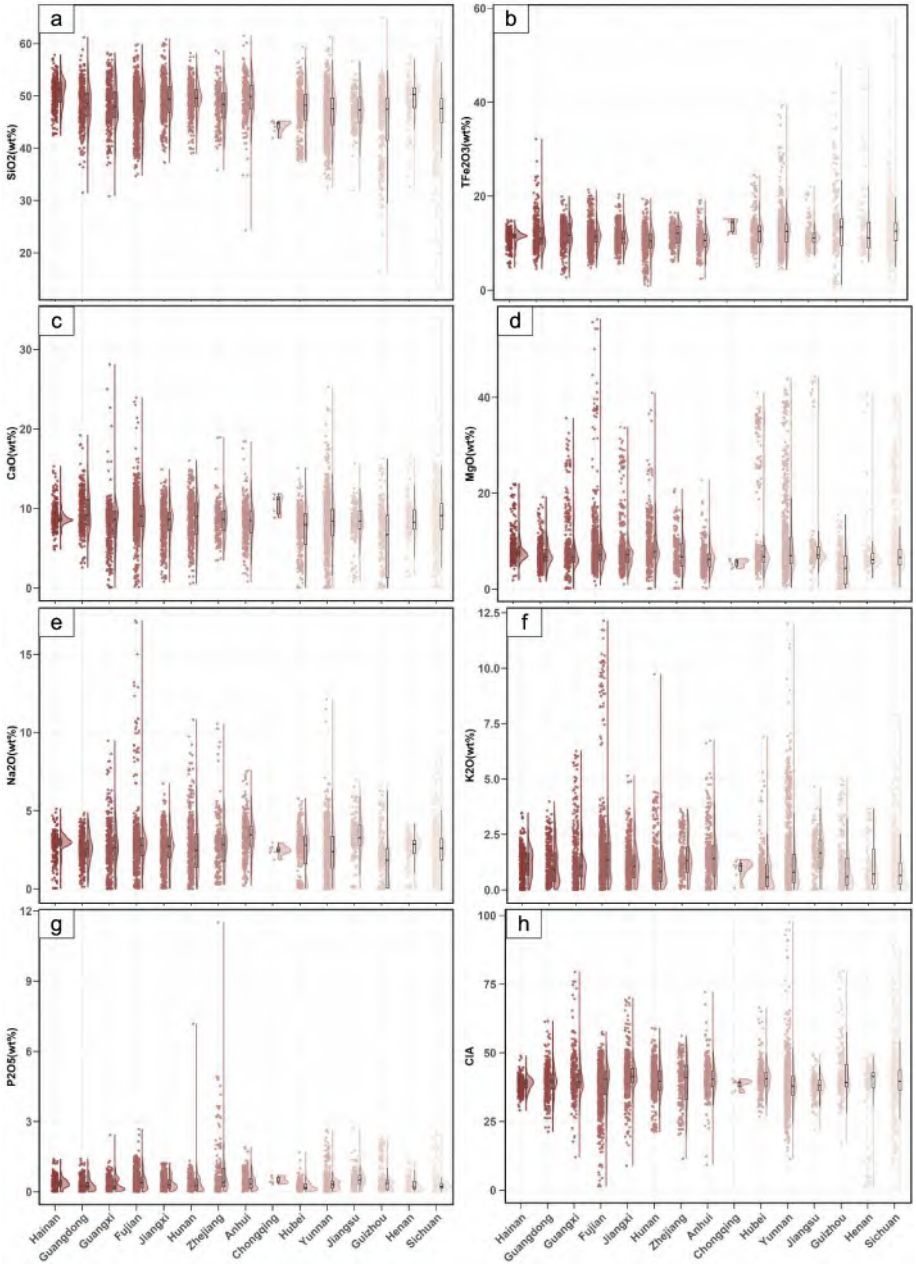

Fig. 4. Major oxide concentrations in rock samples across provinces in South China. Raincloud plots show the distribution of each oxide in each province, with the violin plot (including boxplot) on one side and individual sample points on the other. (a) Silicon oxide (SiO_2, wt%); (b) Total iron oxide (TFe_2O_3, wt%); (c) Carbon oxide (CaO, wt%); (d) Magnesium oxide (MgO, wt%); (e) Sodium oxide (Na_2O, wt%); (f) Potassium oxide (K_2O, wt%); (g) Phosphorus oxide (P_2O_5, wt%); (h) CIA. Color gradients indicate climatic variables: red for mean annual temperature (darker = higher). Data shown comprise the complete compiled dataset from peer-reviewed articles, inclusive of all samples (n = 7, 037) before quality filtering. (For interpretation of the references to color in this figure legend, the reader is referred to the Web version of this article.)

characterized using standard visualization techniques, including major element variation diagrams (Fig. 4; Figs. S5 and S6) and trace element spatial distribution diagrams (Fig. 5; Fig. S7).

To exclude weathered or hydrothermally altered samples, the loss-on-ignition (LOI) and Chemical Index of Alteration (CIA) values were considered for the data filtering process. CIA = [$Al_2O_3/(Al_2O_3 + K_2O + CaO^* + Na_2O) \times 100$] in molecular proportions where CaO* represents calcium hosted in silicate minerals (Fu et al., 2023; McLennan, 1993). As bulk mineralogical data were unavailable for most samples, the reported CaO value was used as the proxy for CaO*. Samples were then filtered by rock type: ultramafic to mafic samples ($SiO_2 < 52$ wt%) with CIA >60 were excluded, and a small number of intermediate rocks ($SiO_2 \geq 52$ wt %) with CIA >80 were similarly removed. Annual precipitation and mean annual temperature for each sample locality were extracted from the ERA5-Land climatological raster dataset via spatial overlay. A subset of samples (n = 258 for the main dataset; n = 150 for the coastal dataset) returned the ArcGIS/QGIS NoData sentinel value (-3.40×10^{38}, the float32 minimum) owing to their position in raster cells flagged as missing coverage. Rather than discarding these geochemically valid samples, missing climate values were recovered through spatial interpolation. For each affected sample, the ten nearest neighbours with valid climate records were identified using a k-d tree constructed on decimal-degree coordinates, and a weighted mean was computed by Inverse Distance Weighting (IDW) with a distance-decay exponent of two (Shepard, 1968):

$$\hat{z}_0 = \frac{\sum_{i=1}^{k} d_{0i}^{-p} z_i}{\sum_{i=1}^{k} d_{0i}^{-p}}$$

where $\hat{z}_0$ is the estimated climate value at the target location, z_i and d_{0i} are the observed value and Euclidean distance of the i-th neighbour respectively, $k = 10$, and $p = 2$. IDW was preferred over global substitution (e.g., dataset mean or median) because precipitation and temperature exhibit strong positive spatial autocorrelation at the regional scale; locally weighted estimates therefore provide a more physically representative approximation than a single global statistic.

For the whole dataset, a total of 7029 rock analyses were initially compiled (8 serpentinised harzburgites or serpentinites removed). After applying the LOI threshold (≤2 wt%), data of 3427 samples were retained (3602 removed). Subsequent CIA-based alteration screening removed a further 230 mafic samples ($SiO_2 < 52$ wt%, CIA >60), yielding 3197 samples; no intermediate to felsic samples exceeded the CIA >80 threshold. An additional 288 samples were excluded owing to missing values in the variables required to compute the rock suitability indicators (SiO_2, TFe_2O_3, MgO, CaO), leaving a final analytical dataset of 2909 samples (Table S3).

For the coastal dataset, all 2634 initially compiled samples possessed complete records for the required rock and distance indicators (W, N, H, D), so no samples were removed at the missing-value screening stage. CIA alteration screening subsequently removed 7 mafic samples ($SiO_2 < 52$ wt%, CIA >60), yielding a final coastal analytical dataset of 2627 samples.

3.3. Methods of rock resource evaluation for ERW

To avoid the influence of subjective opinions and deviation from real implementation scenarios, we combined the subjective and objective weight allocation methods of various indices to form a primary and data-based evaluation framework (Table 2). While a comprehensive ERW rock resource evaluation ideally considers numerous factors such as rock type, total resource volume, local natural soil conditions, energy costs, and human policy, detailed data are often unavailable or the comprehensive influences that heavy metals and nutrients have on plants and animals are unclear at this early research stage. Therefore, we narrowed down to three decision criteria through a subjective process to avoid overcomplicating the initial evaluation (Fig. 6), including Rock Index,

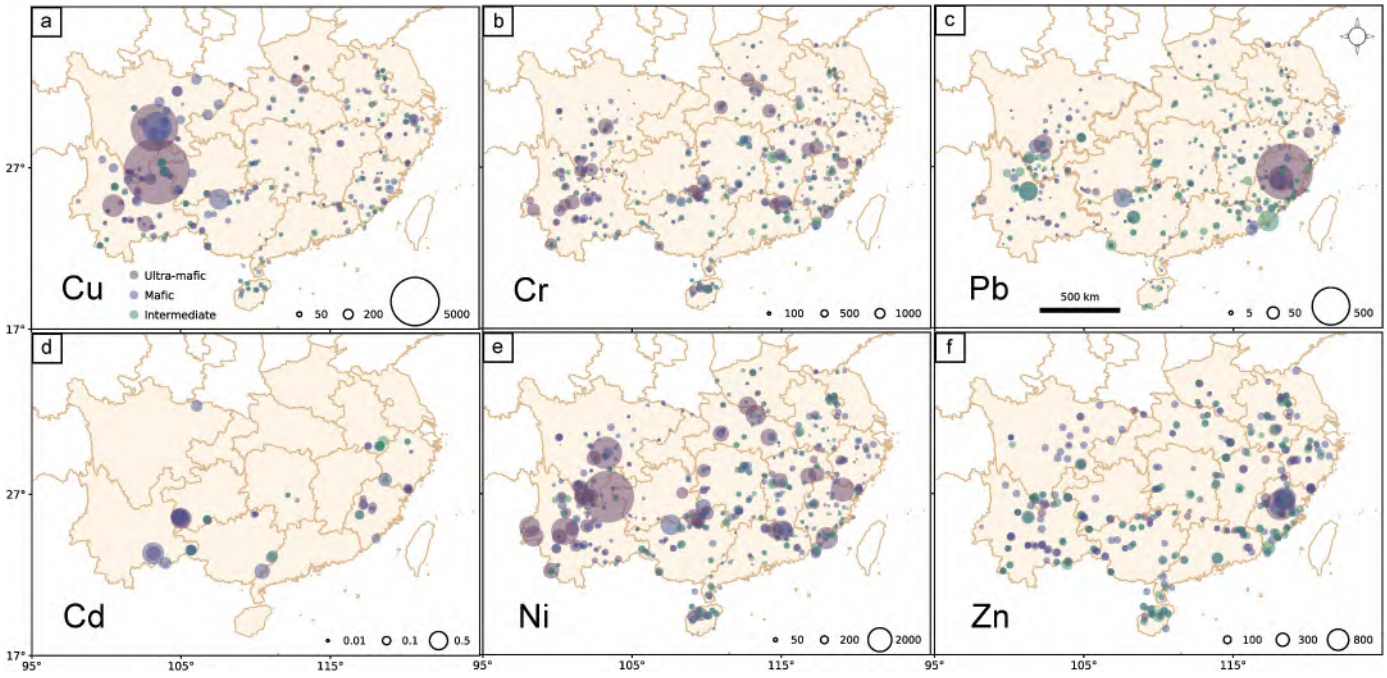

Fig. 5. Spatial distribution and clustering of heavy metal concentrations (in ppm) in rock samples separating into different groups according to SiO_2 content (<45% for ultra-mafic rocks, 45–52% for mafic rocks and >52% for intermediate rocks). The study area is divided into 0.7° × 0.7° grids, and symbol sizes represent the average concentration of each metal within each grid cell. Circle size is calculated as: Marker size ∝ (mean concentration × scaling factor). The applied scaling factors are: Cu × 0.5, Cr × 0.10, Cd × 700.00, Pb × 3.00, Ni × 0.30, Zn × 0.60.
(a) Copper (Cu); (b) Chromium (Cr); (c) Cadmium (Cd); (d) Lead (Pb); (e) Nickel (Ni); (f) Zinc (Zn). Note that the data shown comprises the complete compiled dataset from peer-reviewed articles, inclusive of all samples before quality filtering.

Table 2
Index names and descriptions of the ERW multi-criteria evaluation framework, categorized by geochemical properties (Rock Index), environmental conditions (Site Index), and data reliability (Sampling Index).

Index Name	Sub-Index	Description
Rock Index	Weathering (W)	Geochemically defined rate and completeness of mineral dissolution; higher values indicate faster and more thorough weathering.
	Nutrients (N)	Content of bioavailable elements (e.g., Na, K, P); higher values enhance ERW effectiveness.
	Heavy Metals (Optional) (H)	Concentration of potentially toxic elements; higher values may pose environmental risks.
Site Index	Temperature (T)	Higher temperatures favor faster mineral dissolution and ERW reactions.
	Precipitation (P)	Local moisture and runoff, which enhance weathering rates.
	Transport Distance (Optional) (D)	Distance from source to deployment site, affects ERW cost, particularly for coastal applications.
Sampling Index (Optional)		Number and spatial distribution of samples per province; higher coverage improves reliability of the evaluation.

Site Index and Sampling Index (also known as study intensity).

To objectively determine the relative importance of the diverse geochemical indicators in assessing rock suitability for ERW applications, an inter-criteria correlation (CRITIC) method (Diakoulaki et al., 1995) was employed. This data-driven approach is particularly robust for geochemical datasets as it quantifies the intrinsic significance of each indicator by simultaneously evaluating its inherent variability and its informational conflict with other criteria, thereby maximizing the unique and non-redundant information extracted from the rock samples. The steps of the CRITIC method to determine the weight of sub-criteria are as follows (Diakoulaki et al., 1995; Odu, 2019):

For positive criterion $x_{ij}^{'}$:

$$x_{ij}^{'} = \frac{x_{ij} - \min(x_j)}{\max(x_j) - \min(x_j)} \tag{1}$$

Here, x_{ij} denotes the value of the j-th geochemical indicator for the i-th rock sample, where $i = 1, \ldots, n$ represents individual samples and $j = 1, \ldots, m$ represents different evaluation indicators.

For negative criterion $x_{ij}^{''}$:

$$x_{ij}^{''} = \frac{\max(x_j) - x_{ij}}{\max(x_j) - \min(x_j)} \tag{2}$$

We use the standard deviation S_j to represent variability of $\overline{X_j}$:

$$S_j = \sqrt{\frac{1}{n-1}\sum_{i=1}^{n}(x_{ij} - \overline{X_j})^2}, \overline{X_j} = \frac{1}{n}\sum_{i=1}^{n} x_{ij} \tag{3}$$

The prominence of an indicator is represented by the symbol V_j:

$$V_j = \sum_{i=1}^{n}(1 - r_{ij}) \tag{4}$$

Where r_{ij} is the correlation coefficient given by:

$$r_{ij} = \frac{\sum_{k=1}^{n}(x_{ki} - \overline{X_i})(x_{kj} - \overline{X_j})}{\sqrt{\sum_{k=1}^{n}(x_{ki} - \overline{X_i})^2}\sqrt{\sum_{k=1}^{n}(x_{kj} - \overline{X_j})^2}} \tag{5}$$

The CRITIC weight is determined by the product of the variability S_j and prominence V_j of an indicator:

$$C_j = S_j \times V_j \tag{6}$$

Finally, the CRITIC weights w_j are normalized so that their sum equals one:

$$w_j = \frac{C_j}{\sum_{j=1}^{m} C_j} \tag{7}$$

In the "Rock Index" sub-criterion, there are three components that need further division.

"Weathering" is represented by the major compositional elements of fast-weathered minerals (e.g., olivine and Ca-plagioclase), which are Si, Fe, Mg and Ca. The carbon capture and dissolution potential are calculated:

$$rev_{SiO_2} = Max_{SiO_2} + Min_{SiO_2} - \%SiO_2 \tag{8}$$

$$W = \left(\frac{\%TFe_2O_3}{M_{TFe_2O_3}} + \frac{\%MgO}{M_{MgO}} + \frac{\%CaO}{M_{CaO}}\right) \times \left(\frac{rev\_SiO_2 - Min_{rev\_SiO_2}}{Max_{rev\_SiO_2} - Min_{rev\_SiO_2}}\right) \tag{9}$$

It should be noted that the "Weathering" Index defined here does not quantify the degree of chemical weathering of the source rock (e.g., CIA), but instead represents its potential weatherability and CO_2 consumption capacity during enhanced rock weathering.

Here, "Nutrients" refers to elements that may contribute to agricultural or nutritional benefits rather than strictly essential plant nutrients:

$$N = \left(\frac{\%Na_2O}{M_{Na_2O}} + \frac{\%K_2O}{M_{K_2O}} + \frac{\%P_2O_5}{M_{P_2O_5}}\right) \tag{10}$$

"Heavy Metals" represents those trace metals that could harm plants, animals and human in general:

$$H = \left(\frac{Cr}{M_{Cr}} + \frac{Co}{M_{Co}} + \frac{Ni}{M_{Ci}} + \frac{Cu}{M_{Cu}} + \frac{Zn}{M_{Zn}} + \frac{Hg}{M_{Hg}} + \frac{Ag}{M_{Ag}} + \frac{Cd}{M_{Cd}} + \frac{Sn}{M_{Sn}} + \frac{Pb}{M_{Pb}}\right) \tag{11}$$

Although some of the elements included in the Heavy Metal Index (e.g., Ni, Cu, Zn, and Fe) are essential micronutrients for plants, they can become toxic at elevated concentrations, particularly under alkaline soil conditions that may result from ERW applications. In particular, Ni concentrations associated with ultramafic rocks warrant careful monitoring in agricultural applications.

3.4. Assessment strategies for ERW in cropland, forest and coastal regions

For the general assessment (i.e., for croplands or forests) in our study, the weight allocated to each sub-criterion under "Rock Index" is determined based on two scenarios: including or excluding heavy metals. The importance of eliminating the potential risks associated with heavy metals mobilization was highlighted in previous studies (Choi et al., 2021). Another research suggested that accumulated trace metals in the mixing sediments in the ocean from enhanced silicate weathering application on coastal regions could pose risks for benthic biota under certain conditions (Flipkens et al., 2021). Given this uncertainty, our default evaluation frameworks retain heavy metals as a sub-criterion, while the alternative scenario excluding them allows users to explore outcomes where heavy metal risks are considered negligible. In this default scenario, the weights assigned are 39.81% for "Weathering", 29.35% for "Nutrients", and 30.84% for "Heavy Metals", determined by the CRITIC method based on the standard deviation and correlation of the input data. Some studies contend that heavy metals may not be a threat to human health during application, because organisms cannot absorb heavy metals in the kind of form that is provided in the crystal structure of minerals (John and Leventhal, 1995; Haque et al., 2020). In this case, the weights are adjusted to 52.82% for "Weathering" and 47.18% for "Nutrients". Weight allocation for "Site Index" is all

Fig. 6. Hierarchical Weight Distribution of the Multi-criteria Decision Framework (Inner Ring: Decision Criteria; Outer Ring: Sub-criteria with Proportional Allocation). Decision Criteria includes "Rock Index" ("Weathering": including TFe_2O_3 defined as total iron (FeO + Fe_2O_3), "Nutrients", "Heavy Metals"); "Site Index" ("Temperature", "Precipitation", "Transport Distance"); "Sampling Index", represents the number of samples, which is only included in provincial evaluations. "Transport Distance" is calculated as the hub distance from the rock resource location to the nearest coastline and is considered only in the coastal-scale evaluation (see Section 4.3). "Sampling Index" is incorporated exclusively in the provincial-scale assessment (see the following text and figures) to reflect spatial data density and confidence in regional evaluation. The decision criteria are directly allocated through consideration of their importance in the ERW application. Indices related to rock properties are crucial and thus given 80% of the evaluation. Background factors, such as temperature and precipitation of the application area, are considered a part of the system, about 15%. To avoid the deviation caused by the research intensity of certain areas, the data size (i.e., number of previous studies) has been considered as a minor 5% weight in the system.

consistent with 33.73% and 66.27% for "Temperature" and "Precipitation", respectively.

Previous studies suggest that the oceans serve as important implementation sites for ERW. Specifically, olivine is proposed to be added into the ocean to enhance weathering (Köhler et al., 2010), in order to prompt the growth of calcifying organisms and increase the drawdown of atmospheric CO_2. Therefore, in addition to croplands and forests, the potential of rock resources for ERW in coastal regions is also evaluated in this study. As mentioned above, transportation of ground silicate rocks is a crucial factor that needs to be taken into account and thus, rocks within a 300 km buffer area of the coastline are considered for coastal ERW evaluation. The following are the decision criteria. In the "Rock Index" sub-criteria, the allocated weight is 46.02% for "Weathering", 37.52% for "Nutrients" and 16.46% for "Heavy Metals". If we take "Heavy Metals" out of consideration, then it is 51.37% for "Weathering" and 48.63% for "Nutrients". In the "Site Index" sub-criteria, 24.56% for "Temperature", 29.55% for "Precipitation", and 45.88% for "Transport Distance". After removing "Transport Distance", it changes to 52.18% for "Temperature", 47.19% for "Precipitation".

4. Results and discussion

4.1. Overall assessment results of rock resources for ERW in South China

Some evaluation results, excluding the "Site Index", are presented in Fig. 7. The results indicate that the "Rock Index" scales vary between approximately 0.21 to 0.71 in the evaluated result excel file, and 0.30 to 0.50 after spatially average-gridded. If excluding the "Heavy metals",

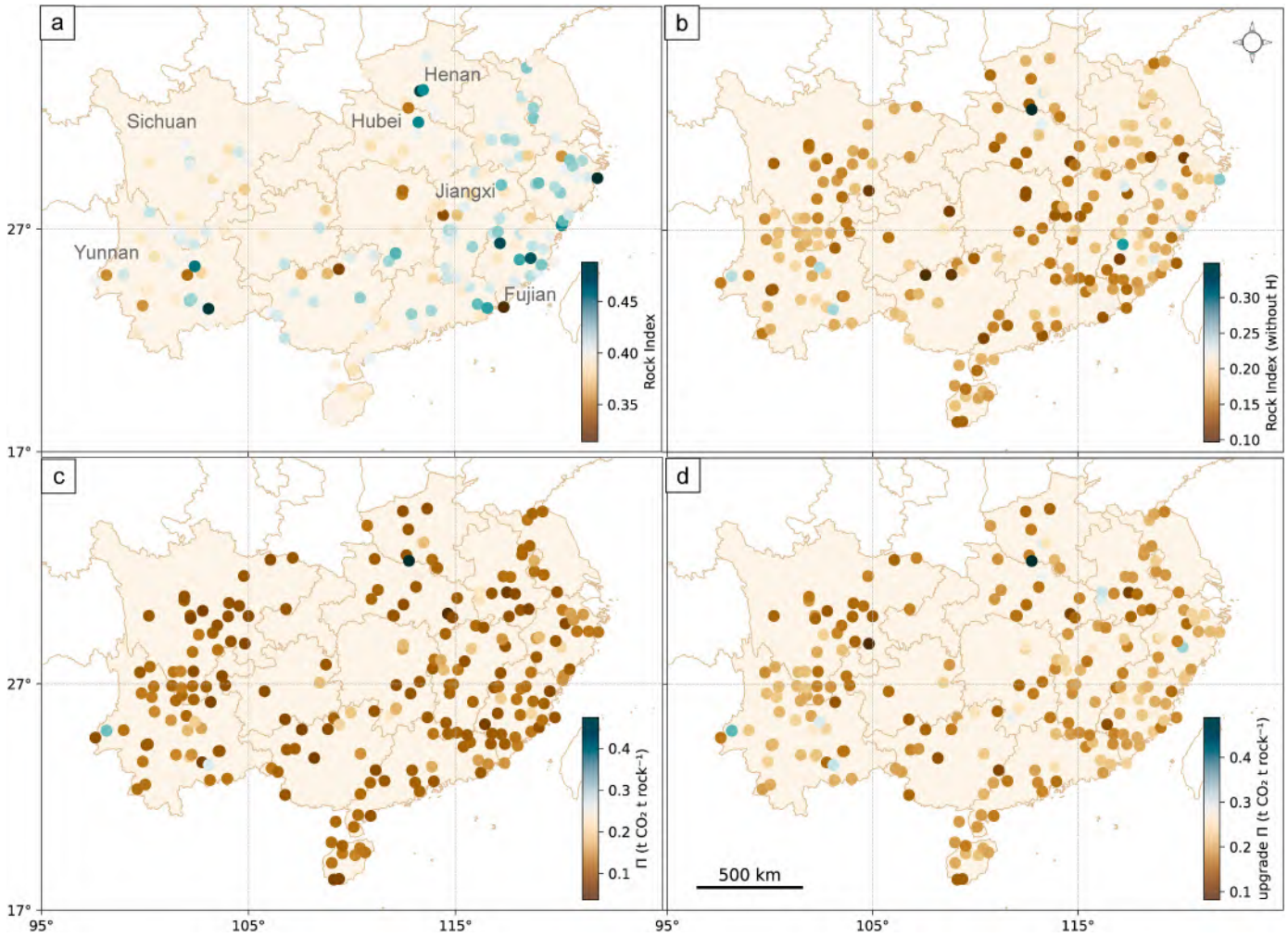

Fig. 7. Rock sample grading (out of 1.0) and Weathering Efficiency (Π) (all 0.7° × 0.7° average-gridded data). Suitability grading for rock samples (a) considering heavy metal content, or (b) ignoring heavy metal content. (c) Weathering Efficiency (Π) (Strefler et al., 2018) based on MgO and TFe_2O_3, representing the theoretical CO_2 capture capacity per unit mass. (d) Modified Π based on CaO, MgO, and TFe_2O_3, for a more comprehensive assessment of carbon removal potential. Note that the rock grading here shares the same grading method as "Rock Index". The grading scale uses a color gradient from brown (low) to green (high). Due to spatial averaging, scores exceeding 0.30 or 0.40 could be categorized as "Highly Suitable", representing the top-tier potential for regional ERW deployment. The shift from raw data (up to 0.71) to gridded data (max ~0.50) reflects the smoothing of localized high-quality outcrops within the 0.7° grid cells. Data used in this figure and the following figures represent the filtered dataset following quality screening and data cleaning (n = 2, 909). (For interpretation of the references to color in this figure legend, the reader is referred to the Web version of this article.)

the scale varies between 0.0048 to 0.68 and 0.10 to 0.35 after spatially average-gridding. To provide an alternative perspective on rock suitability and to cross-validate our evaluation framework, Weathering Efficiency (Π) was also calculated (Strefler et al., 2018). Weathering Efficiency represents the intrinsic capacity of a rock to sequester CO_2 per unit mass, serving as a direct indicator of its chemical reactivity and overall effectiveness in ERW applications. Its calculation results allow for an examination of distribution patterns based purely on inherent weathering potential. As shown in Fig. 7c and d, the distribution patterns derived from this independent metric were found to be largely consistent with those generated by our primary grading method. We notice that the most promising rock resources are located in southern Henan, adjacent areas for Jiangxi and Fujian, central and western Yunnan. By contrast, related less promising ones are in northern Yunnan and Sichuan, and adjacent areas of Jiangxi, Hubei and Hunan (Fig. 7c; 7d).

ERW implementation also needs to consider the background of the performing sites. The results involving "Site Index" are illustrated in Fig. 8. The "Weathering" is calculated to vary from 0.0 to 0.79, then normalized to 0–1. Prominent favorable examples include the Guangdong, Hainan, Fujian, Guangxi, and Jiangxi provinces. Bi-scale graph (Fig. 8a) shows that the southern part of Hubei, Hunan, and Guizhou, appears less ideal for ERW implementation. Additionally, rock resources in Hainan may seem less compatible for ERW despite their favorable climate background due to their low weathering efficiency and relatively high heavy metal concentrations. Conversely, the east coast area of South China emerges as a promising region for ERW. In addition, there are areas of rock resources in Henan Province, the middle of Sichuan Province, northern Yunnan Province that would be quite a good fit for ERW.

As for the consideration of soil benefits and risks, the spatial and linear patterns of "Nutrients" and "Heavy Metals" are shown in Fig. 8b; Fig. S8–S10. Higher values of the nutrient-related index indicate a greater potential to increase soil phosphorus availability (Bi et al., 2024) and to improve or maintain crop nutritional status (Beerling et al., 2024), whereas higher heavy metal index indicates a greater potential risk associated with trace element accumulation (Levy et al., 2024). Regions highlighted in orange represent rock resources with relatively high nutrient benefits and comparatively low heavy metal risks (Fig. 8b), such as central Sichuan and Anhui provinces, and the

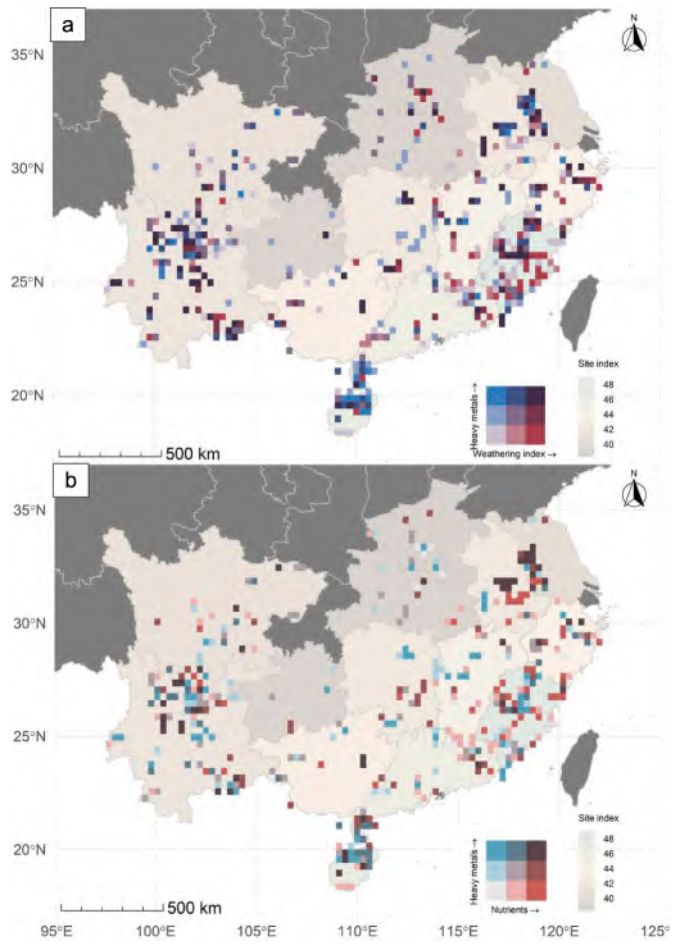

Fig. 8. Spatial clustering 3° × 3° average-gridded bi-scale evaluation of the samples. (a) Joint evaluation of the "Weathering" Index and "Heavy metals" Index: The bivariate legend (3 × 3 matrix) classifies rock resources by their weathering efficiency (x-axis) and heavy metal risk (y-axis). Red/Warm-toned cells represent the "high weathering, low risk" ideal, while blue/cool-toned cells indicate "low weathering, high risk" scenarios; (b) Joint evaluation of "Nutrients" Index and "Heavy metals" Index. "Site Index" is included (consisting of 33.73% for "Temperature", and 66.27% for "Precipitation") as background evaluation (out of 1.00) colormap of each province: The legend classifies resources by nutrient benefit (x-axis) vs. heavy metal risk (y-axis). Orange regions signify premium feedstocks (high nutrient, low risk), whereas green regions highlight contamination hotspots (low nutrient, high risk). Higher values of the "Weathering" and "Nutrients" indices indicate faster-weathering and more nutrient-beneficial feedstocks, respectively, whereas higher "Heavy Metals" Index values indicate greater potential environmental risk. The figure presents a comparative evaluation across provinces rather than a selection of a single "best" rock type. The underlying map colors represent the Site Index (0.0–1.0), where greener colors indicate optimal environmental conditions (high temperature and precipitation) for Enhanced Rock Weathering (ERW). (For interpretation of the references to color in this figure legend, the reader is referred to the Web version of this article.)

southeastern coastal areas of Fujian and Zhejiang provinces. In contrast, green-colored regions (largely distributed in Yunnan Province and Hainan provinces, Fig. 8b) indicate relatively higher heavy metal risks, which should be carefully considered or avoided during implementation.

From the regional perspective, in order to propose the most favorable locations for practical ERW implementation, each province is regarded as an evaluation unit and the comprehensive provincial evaluation results are shown in Fig. 9. These results show that the southern areas of South China are high-potential provinces. These provinces have various gradings in an interval of approximately 10 to 12 points differences between the best and the least suitable provinces for ERW. The Fujian Province demonstrates the highest potential for ERW implementation, followed by Hainan, Guangdong, Jiangxi and Zhejiang provinces as strong contenders. From only considering the potential of rock resources, Henan Province holds great potential from our evaluation and previous model simulation (Guo et al., 2023). The Sichuan Province is ranked last mainly because of its low annual temperature and rainfall.

4.2. Distributions of the high-potential rocks for ERW

The descriptions of the most high-potential rocks for ERW in South China (Fig. 10), involving locations, ages, mineral compositions and petrogenesis, are shown in Table 3. Note that serpentinised ultramafic rocks that may contain asbestos are filtered out before evaluation, because grinding and spreading ultramafic rocks can generate inhalable fibers that cause cancer and fibrosis, with no known safe exposure threshold (Lee et al., 2008; Marzini et al., 2024).

The magnetite pyroxenite hosted within the Tieshanmiao-type iron deposits at Tieshan mining area, Wugang, Henan Province (Fig. 10b) represents a Neoarchean (ca. 2.7–2.5 Ga) lithology. It is predominantly comprised of pyroxene (65%) and magnetite (35%), with accessory calcite, quartz, and apatite (<5%), and its genesis is attributed to metamorphosed quartz-carbonate iron formations (Yao et al., 2015). Another significant resource is the ELIP, particularly the large mafic intrusions situated around Panzhihua and Hongge in Sichuan Province (Fig. 10c). These Permian (ca. 260 Ma) cumulates, typically consisting of clinopyroxene (50%), plagioclase (40%), olivine (<12%), magnetite, and hornblende, represent late-stage differentiates derived from the fractionation of tholeiitic or picritic magmas in a plutonic setting (Zhou et al., 2005; Luan et al., 2014). Their substantial volume, exemplified by the Hongge intrusion (about 96–192 km^3), underscores their significant potential for ERW. In Jiangsu Province, spinel-lherzolite xenoliths entrained within Pleistocene alkali basalts at Panshishan (Fig. 10d) constitute a key target. Composed of olivine, orthopyroxene, clinopyroxene, and spinel, these xenoliths are interpreted as refractory mantle residues following varying degrees of partial melting (Huang et al., 2013a). Additionally, the Cretaceous harzburgite from Changji, Putian, Fujian Province (Fig. 10e), offers high coastal potential. The harzburgite body is predominantly composed of olivine, is interpreted as a tectonic slice of mantle peridotite emplaced into the crust (Chen and Zeng, 1983). Further high-potential ultramafic rocks are found in Zhenghe, Fujian Province (Fig. 10e). These Late Sinian to Early Paleozoic rocks, consisting of olivine, orthopyroxene, and clinopyroxene, are interpreted as a mélange comprising melt-extracted residual mantle and ultramafic cumulates, likely formed during the Late Sinian to Early Paleozoic before subsequent tectonic emplacement, alteration, and metamorphism (Ren et al., 1997). The high potential of these rocks for ERW is often intrinsic to their mafic or ultramafic nature and, in specific instances, their metamorphic history. While not exclusively metamorphic, these high-potential reservoirs are consistently associated with tectonically active zones or metallogenic belts characterized by abundant ferromagnesian minerals.

Furthermore, Cenozoic mafic volcanic rocks, including foidite, picrobasalt, basanite, and basalt, are widely distributed, particularly along the southern coast (e.g., Hainan and Guangdong Province, covering over 4000 km^2; Huang et al., 2013b; Zhou et al., 2021). Their basic composition suggests high potential for ERW. Their widespread distribution and relatively young age make them highly accessible resources, refer to the following subsection 4.3 for more detailed explanations.

4.3. High-potential rock resources for ERW in South China coastal regions

Based on the evaluation results of coastal ERW rock resources (Fig. 11; Fig. S11), the southeastern coastline of Fujian and Zhejiang Province is quite suitable for ERW. The rocks in Jiangsu Province are quite far from coast, however, they have low heavy metals and high

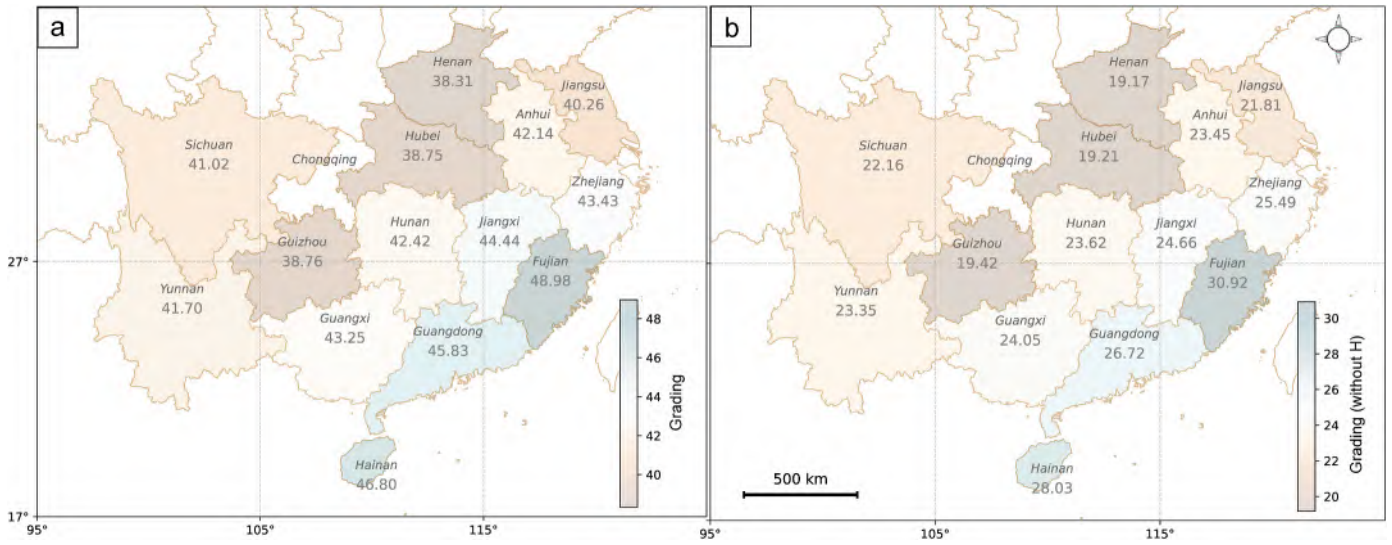

Fig. 9. Grading (out of 100) of whole province (considering 80% for "Rock Index", 15 % for "Site Index" and 5% for "Sampling Index"). In "Rock Index", 39.81% for "Weathering", 29.35% for "Nutrients" and 30.84% for "Heavy Metals"; In "Site Index", 33.73% for "Temperature", 66.27% for "Precipitation". (a) heavy metals considered; (b) heavy metals not considered. Higher gradings indicate more favorable conditions for Enhanced Rock Weathering (ERW) based on climate, local feedstock geochemistry and number of samples. Samples in Chongqing have been filtered out after the process, therefore provincial analysis did not include Chongqing.

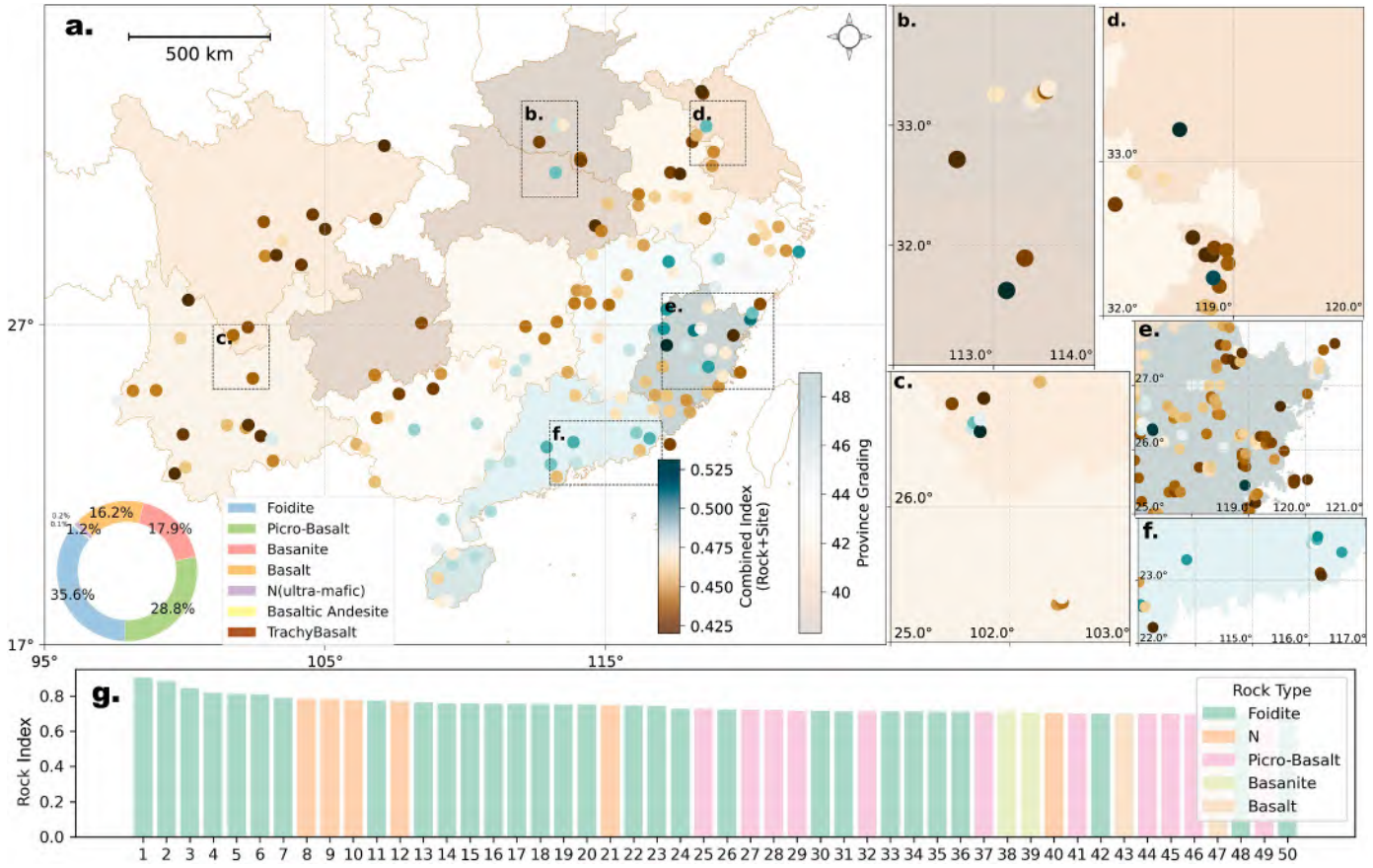

Fig. 10. Spatial 0.7° × 0.7° gridded distribution of high-potential rock resource. (a) Regional-scale distribution based on spatially aggregated results within each grid cell, where each point represents the average evaluation of all rock samples located in that grid rather than individual samples. Panels (b)–(f) show enlarged views of the areas outlined by dashed boxes labeled a., b., c., and d. in panel (a), respectively. (g) Ranking of individual rock samples based on the Rock Index, showing the top 50 samples with the highest index values. These samples are included in the gridded aggregation shown in panel (a) but are not displayed individually due to spatial averaging. Only rock resources with evaluation scores ≥42 are considered as high-potential resources according to the score range. The Combined Index for rock resources is normalized to a range of 0–1.00 and incorporates both "Rock Index" and "Site Index", which accounts for local temperature and precipitation conditions.

Table 3
Mineral compositions, ages and formation process of the high-potential rock resources for ERW.

Location	Rock resources	Ages	Mineral compositions	Petrogenesis
Panzhihua and Hongge, Sichuan	Emeishan Large Igneous Province and its large mafic intrusions [a]	Permian, 260 Ma	Clinopyroxene (50%), plagioclase (40%), olivine (<12%), magnetite and hornblende	Late-stage liquids associated with the fractionation of tholeiitic or picritic magmas in a plutonic setting
Tieshan mining area, Wugang, Henan	Magnetite pyroxenite in Tieshanmiao-type iron deposits [b]	Neoarchean, 2.7–2.5 Ga	Pyroxene (65%) and magnetite (35%), calcite, quartz and apatite	Metamorphosed iron-bearing ultramafic formations
Changji, Putian, Fujian	Harzburgite [c]	Cretaceous	Mostly olivine	Fragment (or slice) of the Earth's mantle, likely emplaced into the crust
Zhenghe, Fujian	Ultramafic rock [d]	Late Sinian to Early Paleozoic	Olivine, orthopyroxene, and clinopyroxene	Mélange of melt-extracted residual mantle and ultramafic cumulates, likely formed during the Late Sinian-Early Paleozoic before subsequent tectonic emplacement, alteration, and metamorphism
Panshishan, Jiangsu	Spinel-lherzolites xenoliths in Cenozoic alkali basalts [e]	Pleistocene	Olivine, orthopyroxene, clinopyroxene and spinel	Residues after different degrees of partial melting from the upper mantle
Jiucaidi, Jieyang, Guangdong	Basalt [f]	Miocene, Neogene, ~20 Ma	Basaltic rocks with few small spinel lherzolite xenoliths, fine-grained plagio clase, clinopyroxene, olivine, and Fe–Ti oxide minerals	Partial melting of the asthenospheric mantle beneath the thickened lithosphere

[a] These rocks were investigated by Zhou et al. (2005) and Luan et al. (2014).
[b] Yao et al. (2015).
[c] Chen and Zeng (1983).
[d] Ren et al. (1997).
[e] Huang et al. (2013a).
[f] Huang et al. (2013b).For the locations, see Fig. 10.

nutrients. In addition, Hainan Province has plenty of Cenozoic basalts that make it great for the implementation of such a strategy. The Cenozoic basalts from Hainan Plume are the subducted Pacific plate crustal materials from the mantle transition zone to the shallow mantle as a result of mantle convection induced by continuous subduction of the Pacific plate. They are porphyritic with phenocrysts of olivine (5–8 vol %) and clinopyroxene (1–4 vol%) (Li et al., 2020). In addition, the Early Paleozoic volcanic rocks on Hainan Island erupted between 446 and 430 Ma (mostly N-MORB-type metabasalts and E-MORB-type metabasalts), and are mainly composed of actinolite, plagioclase, amphibole, albite, chlorite, epidote and pyroxene (Zhou et al., 2021). These rocks, combined with their climatic background, turn out to be great ERW rock resources in coastal regions.

4.4. Suggestions and possible strategies of ERW implementation in South China

For real-world ERW implementation, rock quantity and availability must be investigated for those holding high potential. The ELIP in southwestern China is a significant source of basalt rocks, with estimates suggesting a volume exceeding 3×10^5 km^3 (Xu et al., 2001) and a distribution area greater than 5×10^5 km^2. The mafic intrusions are amongst the best-rated samples in our evaluation. For example, the Panzhihua Fe–Ti–V oxide mine has thus far produced over 134 million tons of ore (Zhou et al., 2005). Additionally, flat Hongge intrusion is about 16 km long, 5~10 km wide and 1.2 km thick (Luan et al., 2014), about 96~192 km^3. The orebodies in Jingshansi mining area are 200–1750 m long, 120–800 m wide, and 23–253 m thick (108 m in average) (Yao et al., 2015), about $2.6 \times 10^6 \sim 1.5 \times 10^8$ m^3. The rock body in southeastern Fujian coast covers about 4 km^2, has 1~3 layers of 40~70 m thick, some parts about 130~150 m thick (Chen and Zeng, 1983). Cenozoic basalts in Hainan cover an area of broader than 4000 km^2 and mainly erupted at 5.5–1.0 Ma (Zhou et al., 2021). All these high-potential rocks are at least 9×10^{14} tons and at least could sequester 2.7×10^{14} t CO_2 if utilized. As the CO_2 emission from energy consumption in 2030 is projected to be $1.02\sim1.25 \times 10^{10}$ t CO_2 yr^{-1} (Huang et al., 2022), the rock amount for ERW should be enough. High-potential resources in several other provinces except for Sichuan, Yunnan and Hainan could be limited for ERW applications, thus industrial waste like slugs could be taken into account as well (Renforth, 2012). Possible strategies for ERW implementation are listed (Table 4) according to local climate, best rock resources, and nearest broad employment area respectively to each high-potential province.

Though Sichuan and Henan Provinces are both rated relatively low in the evaluation results (Fig. 9), mainly because of their climate conditions. However, as the rock evaluation results (Fig. 10) show, some highly promising rock resources existed there. As a result, these two provinces can be incorporated into the possible ERW implementation areas. Environmental regulations in China will also need to be strictly adhered to. The high heavy metal concentrations of rocks in Hainan and central South China should be seriously considered and examined in the future.

ERW field trials and lab experiments have already been conducted at several locations (Table 5; Abdalqadir et al., 2024), with basalt and wollastonite serving as the most frequently tested feedstocks for validating key predictions: (i) measurable carbon sequestration, with basalt trials in the US Corn Belt demonstrating cumulative removal of 10.5 ± 3.8 t CO_2 ha^{-1} (Beerling et al., 2024) and wollastonite trials in Canada showing rapid pedogenic carbonate formation (Haque et al., 2020); (ii) agronomic co-benefits, including crop yield increases of 12–21% and effective mitigation of soil acidification (Kelland et al., 2020; Beerling et al., 2024); and (iii) enhanced nutrient cycling, particularly increased phosphorus availability (Vienne et al., 2022). These field trials provide crucial suggestions for future conduct of ERW in South China, including quantifiable carbon removal rate and co-benefits. From the challenges that previous tests faced (Table 5), the monitoring of soil organic matter and pH is crucial as well.

For large-scale deployment in China, initial implementation should prioritize the provinces and rock resources identified in Table 4. The proposed testing regions encompass croplands, coastal zones, and significant forested areas, which could potentially triple the CDR effect by combining geochemical and biotic carbon removal pathways (Gaucher et al., 2025). As mentioned above, calculation results indicate that the rock resources within the ELIP alone are sufficient to support substantial national-scale CDR.

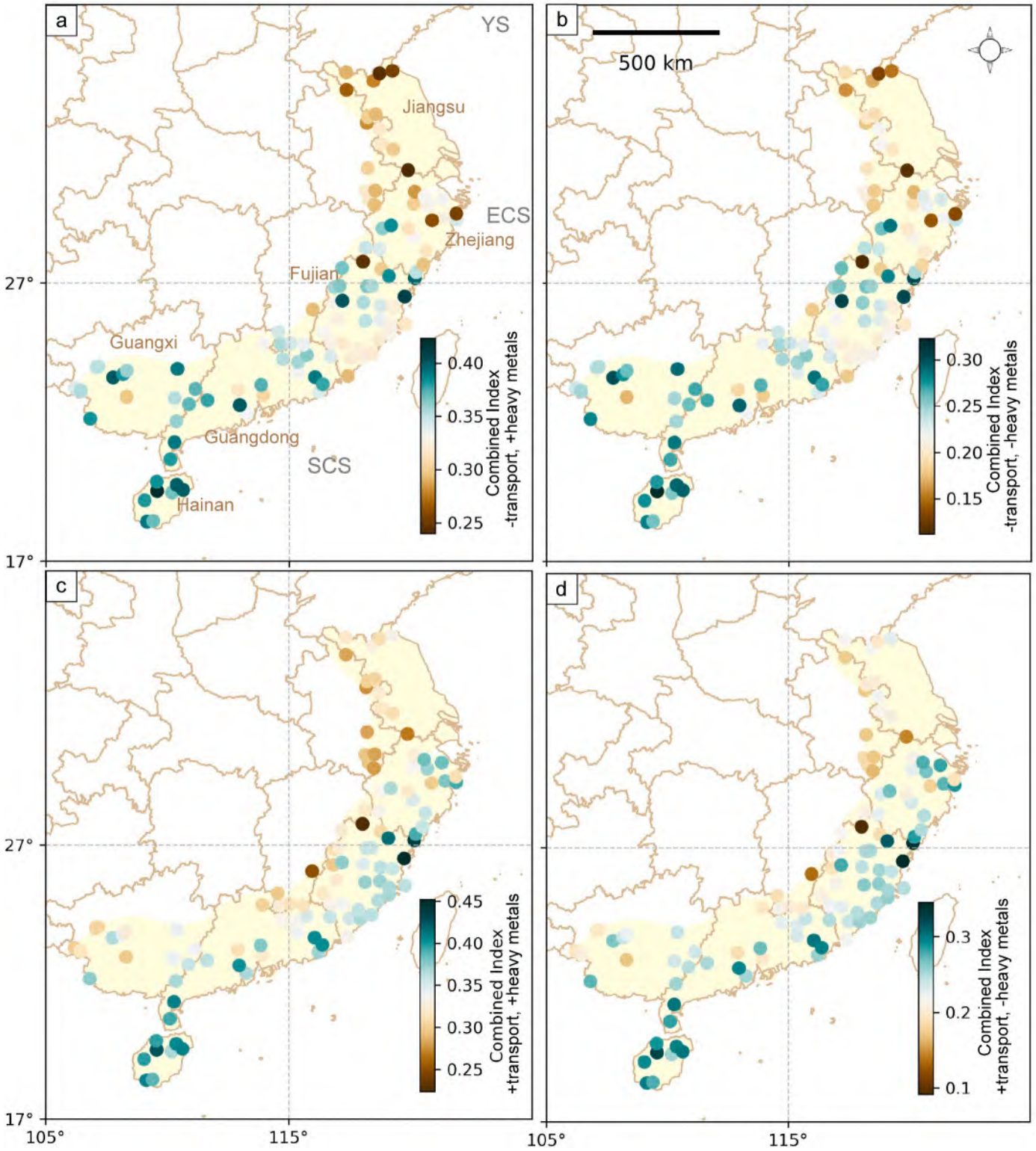

Fig. 11. Assessment (out of 1.0) of Enhanced Rock Weathering suitability in the coastal region 0.7° × 0.7° gridded, considering "Rock Index" and "Site Index". (a) Heavy metals considered, transport distance excluded; (b) Heavy metals excluded, transport distance excluded; (c) Heavy metals considered, transport distance included; (d) Heavy metals excluded, transport distance included. Transport distance is defined as the hub distance from rock resource locations to the nearest coastline and is incorporated only in scenarios where coastal logistics are evaluated. The comparison highlights how environmental risk (heavy metals) and logistical constraints (transport distance) influence the spatial distribution and ranking of potential ERW deployment areas. The calculated evaluation scores exhibited distinct ranges depending on the specific factors considered and whether raw or spatially aggregated data were used. When all factors were included, scores ranged from 0.17 to 0.65 in the raw dataset, narrowing to 0.22 to 0.45 after spatial gridding. Excluding "Heavy Metals", the ranges were 0.0047–0.64 (raw) and 0.10–0.35 (gridded). For scenarios omitting "Transport Distance", scores spanned 0.13–0.69 (raw) and 0.24–0.45 (gridded). Finally, with both "Heavy Metals" and "Transport Distance" excluded, the ranges were 0.004–0.67 (raw) and 0.10–0.35 (gridded). Data used in this figure represent the filtered dataset following quality screening and data cleaning in the coastal setting (n = 2, 627).

Table 4
Possible strategies for the implementation of ERW in high-potential provinces.

Province	Rock resources	Rock volume	Employment area	Heavy metal risks
Yunnan/ Sichuan	Emeishan Large Igneous Province and its large mafic intrusions	$>3 \times 10^5$ km^3	Local forests	Medium
Henan	Magnetite pyroxenite in Tieshanmiao-type iron deposits	$2.6 \times 10^6 \sim 1.5 \times 10^8$ m^3	Croplands covering the whole province except the western area	Low
Fujian	Harzburgite from Cretaceous Pacific Plate subtracting Eurasian Plate; Ultramafic rock from Zhenghe County resulted from Caledonian Orogeny	$1.6 \sim 8.4 \times 10^6$ m^3	Coasal region; Nearby croplands and forests	Medium
Hainan	Cenozoic basalts on the northern island and Early Paleozoic metabasalts outcropped across the whole island[a]	cover an area of broader than 4000 km^2	The whole island includes Croplands and coasts	High
Guangdong	Several episodes of Cenozoic basaltic volcanism along the coast	unreported	East coast; Other croplands and shrublands	Low

[a] These rocks were investigated by Li et al. (2020) and Zhou et al. (2021).

4.5. Implications

Our comprehensive assessment identified high-potential ERW rock resources in South China, particularly within climatically favorable regions and specific lithological units. From a practical standpoint, the detailed figures generated in this study offer actionable insights for policymakers and project developers seeking to deploy ERW in this region. Pinpointing specific provinces such as Fujian, Guangdong, Hainan, Guangxi, and Jiangxi provinces, along with optimal rock types like metamorphosed harzburgite, gabbro, and pyroxenite, enables more targeted resource allocation and infrastructure planning. This specificity can significantly accelerate ERW's adoption as a viable climate mitigation strategy. Our findings directly inform future geological exploration for optimal ERW feedstocks in South China, suggesting promising avenues like targeting magmatic provinces associated with specific tectonic events (e.g., Mesozoic extensional settings for high-quality basalts, or Proterozoic ophiolites for ultramafic rocks) and focusing on rock types with naturally higher proportions of fast-weathering minerals (e.g., olivine and pyroxene). Understanding the petrogenesis and age of these formations will guide more efficient resource exploration. Notably, our analysis indicates that mafic rock that has undergone metamorphism holds the highest potential for ERW in South China. Furthermore, recent researches on crushed wollastonite as an efficient ERW source (te Pas et al., 2023; Yan et al., 2023; Xu et al., 2024), known for inhibiting atmospheric carbon dioxide release in alkaline soils and enhancing soil organic carbon content (Su et al., 2025), suggests an additional rock searching strategy: exploring metamorphic rocks across plate boundaries and orogenic belts, where wollastonite extensively exists in metamorphic limestone or dolomite bodies.

The multi-criteria assessment framework developed and applied in our study possesses significant potential for global upscaling. This methodology, which integrates geological and climatic suitability with environmental safeguards, can be adapted and deployed in other climatically favorable regions worldwide, such as Baturité massif in NE Brazil (Bétard, 2012) and Deccan Traps in India (Das et al., 2005), providing a standardized approach for ERW resource assessment that can contribute to global CDR strategies.

Crucially, this work establishes, for the first time, a comprehensive geochemical database for mafic and ultramafic rocks in South China. Compared to existing global geochemical repositories like PetDB and

Table 5
Global review of reported ERW field trials and their outcomes.

References	Location/ Context	Source Rock	Key CO_2 Findings	Observed Co-Benefits	Encountered Problems/Challenges
Manning et al. (2013)	UK Artificial Soils	Basalt, Dolerite	Demonstrated carbon capture via carbonate precipitation in engineered soils.	Supported the establishment of new plant communities.	N/A.
Haque et al. (2020)	Ontario, Canada Agriculture	Wollastonite-bearing skarns	Demonstrated enhanced carbonation processes and inorganic carbon sequestration in agricultural land.	Improved plant growth and crop yield.	N/A.
Larkin et al. (2022)	Malaysia Oil Palm Plantation	Basalt	Found similar CO_2 drawdown levels in both amended and unamended reference catchments.	N/A.	Difficulty in distinguishing the ERW signal from high background weathering rates.
Sokol et al. (2024)	California, USA Croplands	Meta-basalt	Observed an increase in Soil Inorganic Carbon (SIC) but a significant reduction in the accrual rate of Mineral-Associated Organic Matter (MAOM).	Increased soil pH.	Net soil organic carbon (SOC) and soil organic nitrogen (SON) stocks were lower in amended plots after two years, posing a major challenge for net carbon accounting.
Dupla et al. (2024)	Vineyard fields, Gorgier, Switzerland	Basalt	Substantial weathering and CO_2 removal are detectable with standard proxies	Basalt ERW measurably alters soil biological, physical, and geochemical fertility.	Standard pore-water ERW proxies (pH, EC, DIC, Ca, Mg) showed no significant increase. Elevated Na flagged potential sodification risk.
Holden et al. (2024)	Queensland, Australia	Basalt	Basalt dissolution was dominated by strong acids rather than carbonic acid, constraining Carbon Dioxide Removal (CDR).	Increased soil pH and extractable Mg and Si in the upper soil layer. No crop yield increase detected.	Strongly acidic soil conditions limited carbonic-acid-driven weathering and were thought to hinder CDR.
Blanc-Betes et al. (2021); Kantola et al. (2023); Beerling et al. (2024)	The United States Corn Belt, Illinois, USA	Basalt	From the combined loss of cation (Ca^{2+} and Mg^{2+}) over 4 years, the speculated CDR potential is 10.5 ± 3.8 t CO_2 ha^{-1}.	Crop yield, micro- and macronutrient concentrations increased with elevated soil fertility and alkalinity. N2O emissions were reduced.	N/A

GEOROC (Gard et al., 2019), which focus on oceanic or large-scale volcanic settings, this new dataset offers denser spatial coverage, more complete metadata, and region-specific geochemical information. It therefore provides a more targeted and versatile foundation not only for ERW assessment, but also for future research in areas such as subsurface CO_2 storage in basaltic rocks (Aradóttir et al., 2012;Matter et al., 2016), geochemical baseline studies (Johnson et al., 2005; Sun et al., 2023), and the exploration of other basalt applications (e.g., basalt fibers; Jamshaid and Mishra, 2016).

4.6. Limitations and scope for future work

Although this work provides a regional-scale screening framework for ERW suitability, we realize there are several limitations that may restrict its applicability to site-specific deployment decisions. These points need to be considered in future ERW studies.

First, soil properties were not explicitly incorporated into the current evaluation framework, despite their strong control on ERW effectiveness. Soil pH and buffering capacity regulate both the magnitude and rate of alkalinization following ERW (Van Der Bauwhede et al., 2024), with strongly buffered or calcareous soils showing limited additional pH increase and reduced carbon dioxide removal potential (Levy et al., 2024). Soil texture, drainage, and hydrological regime further influence gas exchange, solute transport, and alkalinity export (Deng et al., 2023), while soil organic matter, roots, and microbial activity can enhance mineral dissolution through biogenic CO_2 supply and organic ligands (Dupla et al., 2024; Lan et al., 2025; Boito et al., 2025; Xu et al., 2025). The omission of these soil-related controls limits the ability of the present framework to predict weathering rates, CO_2 uptake, and co-benefits at the field scale.

Second, the assessment of rock suitability was based primarily on bulk geochemical composition, without explicit consideration of asbestos content or modal mineralogy. While bulk chemistry provides a useful first-order proxy at regional scales, modal mineralogy more directly constrains weathering kinetics and reactive surface availability. Future work should therefore integrate mineralogical data and alteration indices to better capture variations in weathering behavior and environmental risk. Present mineralogical data is limited by the specific research objectives of originally published studies (e.g., tectonic revolution does not specifically require modal mineralogical data detection). Modal mineralogy index will be considered in the improved evaluation framework if sufficient data is provided in the future.

Third, not all the collected data of the rock samples include determined CO_2 content, making it difficult to determine whether the rocks contain trace calcite. While carbonates weather significantly faster than silicates, they may offer lower net carbon removal efficiency. Without precise carbonate quantification, the long-term carbon-sink potential of silicate-based feedstock may be subject to higher uncertainty.

Fourth, the CIA values were calculated using total CaO rather than CaO*, which represents Ca derived only from the silicate fraction, due to the lack of mineralogical data. And the selection of the LOI and CIA thresholds was subjective. These empirical determinations may introduce uncertainty into the evaluation results. Deep in-situ carbonation is a separate CDR technology that could benefit from this dataset, which is represented by McGrail et al. (2017) field trial, in which 40 megatons of preheated CO_2 per day were injected into subsurface basalt rocks at depths of 828–887 m below the surface. Particularly, it would require a different decision scheme considering opportunities and life-cycle analyses for drilling, delivering and injecting CO_2 into subsurface rocks. Future work would also benefit from more localized, high-resolution sampling and in-situ field trials to validate weathering and CO_2 removal rates and heavy metal release in real-world conditions. Expanding the assessment to include other environmental parameters, such as biodiversity impact or water availability constraints, may provide an even more holistic view. Furthermore, integrating economic modeling to assess the cost-effectiveness and scalability of ERW in the identified promising regions represents a vital next step for practical implementation (Zhang et al., 2023).

5. Conclusions

Our study successfully addresses its primary aims by establishing a robust geochemical database for 7037 mafic and ultramafic rock samples across South China Through a multi-criteria evaluation considering rock characteristics, environmental factors, and data reliability, we propose that the Fujian Province is the optimal location for ERW implementation (with its Cretaceous and Cenozoic mafic rocks), with Guangdong, Jiangxi, and Hainan provinces identified as highly suitable alternatives. The Emeishan Igneous Large Province in southwestern China, the iron-bearing pyroxenite in Henan Province and Cenozoic basaltic rock in Fujian, Guangdong and Hainan Province show great potential for ERW rock resources. Additionally, the coastlines of Guangdong and Hainan Province are ideal sites for coastal ERW. We highlight that the heavy metal elements like copper, cadmium, and lead require careful consideration for environmental impact, emphasizing the need to further refine risk assessment based on their hazardous concentrations. Our study provides a practical framework for ERW resource utilization and deployment that is not only applicable to climatically favorable regions in South China but also scalable for a global assessment. This methodology can be further refined by incorporating mineral compositions, which primarily govern rock chemical behaviors, for even more precise evaluations. Our findings contribute to a deeper understanding of ERW application, supporting global carbon removal efforts through data-driven and spatially explicit resource management.

CRediT authorship contribution statement

Shan Qi: Conceptualization, Data curation, Formal analysis, Methodology, Visualization, Writing – original draft, Writing – review & editing. **Xing Jian:** Funding acquisition, Supervision, Writing – review & editing.

Declaration of competing interest

The authors declare that they have no known competing financial interests or personal relationships that could have appeared to influence the work reported in this paper.

Acknowledgements

This work is supported by the National Natural Science Foundation of China (No. 42476051) and the Open Innovation Fund for undergraduate students of Xiamen University (KFJJ-202418). We would like to thank graduate students Hanjing Fu and Xiaotian Shen at Xiamen University for their help and suggestions on graphing. We are really grateful to the editor and two anonymous reviewers for their thoughtful and constructive comments on this manuscript. Furthermore, we acknowledge the support from the Ocean Science Honorary Program for undergraduate students at Xiamen University, which provided a stimulating academic environment for this research.

Appendix A. Supplementary data

Supplementary data to this article can be found online at https://doi.org/10.1016/j.apgeochem.2026.106812.

Data availability

The data (Tables S1, S2 & S3) and original code that support the findings of this study are openly available in the Open Science Framework at https://doi.org/10.17605/OSF.IO/PHTV6.

References

Abdalqadir, M., Hughes, D., Rezaei Gomari, S., Rafiq, U., 2024. A state of the art of review on factors affecting the enhanced weathering in agricultural soil: strategies for carbon sequestration and climate mitigation. Environ. Sci. Pollut. Control Ser. 31 (13), 19047–19070.

Ali, A., Kakar, M.I., El-Ghali, M.A., Rehman, H.U., Abbasi, I.A., Moustafa, M., 2025. Experimental studies on CO2 sequestration via enhanced rock weathering in seawater: insights for climate change mitigation strategies in coastal and open ocean environments. Acta Geochimica 44 (3), 496–512.

Ali, J.R., Thompson, G.M., Zhou, M.F., Song, X., 2005. Emeishan large igneous province, Southwest China. Lithos 79 (3–4), 475–489.

Aradóttir, E.S.P., Sonnenthal, E.L., Björnsson, G., Jónsson, H., 2012. Multidimensional reactive transport modeling of CO_2 mineral sequestration in basalts at the Hellisheidi geothermal field, Iceland. Int. J. Greenh. Gas Control 9, 24–40.

Baker, H.S., Millar, R.J., Karoly, D.J., Beyerle, U., Guillod, B.P., Mitchell, D., Shiogama, H., Sparrow, S., Woollings, T., Allen, M.R., 2018. Higher CO_2 concentrations increase extreme event risk in a 1.5 °C world. Nat. Clim. Change 8, 604–608.

Bayon, G., Patriat, M., Godderis, Y., Trinquier, A., De Deckker, P., Kulhanek, D.K., Holbourn, A., Rosenthal, Y., 2023. Accelerated mafic weathering in Southeast Asia linked to late Neogene cooling. Sci. Adv. 9 (13) eadf3141.

Bazzaz, F.A., 1990. The response of natural ecosystems to the rising global CO_2 levels. Annu. Rev. Ecol. Systemat. 167–196.

Beck, H., Zimmermann, N., McVicar, T., Vergopolan, N., Berg, A., Wood, E.F., 2018. Present and future Köppen-Geiger climate classification maps at 1-km resolution. Sci. Data 5, 180214.

Beerling, D.J., Epihov, D.Z., Kantola, I.B., Masters, M.D., Reershemius, T., Planavsky, N. J., Reinhard, C.T., Jordan, J.S., Thorne, S.J., Weber, J., Val Martin, M., Freckleton, R. P., Hartley, S.E., James, R.H., Pearce, C.R., DeLucia, E.H., Banwart, S.A., 2024. Enhanced weathering in the US Corn Belt delivers carbon removal with agronomic benefits. Proc. Natl. Acad. Sci. 121 (9), e2319436121.

Beerling, D.J., Kantzas, E.P., Lomas, M.R., Wade, P., Eufrasio, R.M., Renforth, P., Sarkar, B., Andrews, M.G., James, R.H., Pearce, C.R., Mercure, J., Pollitt, H., Holden, P.B., Edwards, N.R., Khanna, M., Koh, L., Quegan, S., Pidgeon, N.F., Janssens, I.A., Hansen, J., Banwart, S.A., 2020. Potential for large-scale CO_2 removal via enhanced rock weathering with croplands. Nature 583 (7815), 242–248.

Beerling, D.J., Leake, J.R., Long, S.P., Scholes, J.D., Ton, J., Nelson, P.N., Bird, M., Kantzas, E., Taylor, L.L., Sarkar, B., Kelland, M., DeLucia, E., Kantola, I., Müller, C., Rau, G., Hansen, J., 2018. Farming with crops and rocks to address global climate, food and soil security. Nat. Plants 4 (3), 138–147.

Belda, M., Holtanová, E., Halenka, T., Kalvová, J., 2014. Climate classification revisited: from Köppen to Trewartha. Clim. Res. 59 (1), 1–13.

Bertagni, M.B., Porporato, A., 2022. The carbon-capture efficiency of natural water alkalinization: implications for enhanced weathering. Sci. Total Environ. 838 (Part 4), 156524.

Bi, B., Li, G., Goll, D.S., Lin, L., Chen, H., Xu, T., Chen, Q., Li, C., Wang, X., Hao, Z., Fang, Y., Yuan, Z., Lambers, H., 2024. Enhanced rock weathering increased soil phosphorus availability and altered root phosphorus-acquisition strategies. Glob. Change Biol. 30 (5), e17310.

Blanc-Betes, E., Kantola, I.B., Gomez-Casanovas, N., Hartman, M.D., Parton, W.J., Lewis, A.L., Beerling, D.J., DeLucia, E.H., 2021. In silico assessment of the potential of basalt amendments to reduce N2O emissions from bioenergy crops. GCB Bioenergy 13 (1), 224–241.

Boito, L., Steinwidder, L., Rijnders, J., Berwouts, J., Janse, S., Niron, H., Roussard, J., Vienne, A., Vicca, S., 2025. Enhanced rock weathering altered soil organic carbon fluxes in a plant trial. Glob. Change Biol. 31 (8), e70373.

Brantley, S.L., 2008. Kinetics of mineral dissolution. In: Kinetics of water-rock Interaction. Springer New York, New York, NY, pp. 151–210.

Bétard, F., 2012. Spatial variations of soil weathering processes in a tropical mountain environment: the Baturité massif and its piedmont (Ceará, NE Brazil). Catena 93, 18–28.

Buckingham, F.L., Henderson, G.M., Holdship, P., Renforth, P., 2022. Soil core study indicates limited CO_2 removal by enhanced weathering in dry croplands in the UK. Appl. Geochem. 147, 105482.

Calabrese, S., Wild, B., Bertagni, M.B., Bourg, I.C., White, C., Aburto, F., Cipolla, G., Noto, L.V., Porporato, A., 2022. Nano-to global-scale uncertainties in terrestrial enhanced weathering. Environ. Sci. Technol. 56 (22), 15261–15272.

Chen, C.H., Lee, C.Y., Shinjo, R., 2008. Was there Jurassic paleo-Pacific subduction in South China?: constraints from $^{40}Ar/^{39}Ar$ dating, elemental and Sr-Nd-Pb isotopic geochemistry of the Mesozoic basalts. Lithos 106 (1–2), 83–92.

Chen, Y.A., Zeng, W.F., 1983. Di man sui kuai—Putian Changji Chaobuxing Yanti [Mantle fragments—The Putian Changji ultramafic rock body]. Fujian Geology (2), 49–56.

Choi, W.J., Park, H.J., Cai, Y., Chang, S.X., 2021. Environmental risks in atmospheric CO_2 removal using enhanced rock weathering are overlooked. Environ. Sci. Technol. 55 (14), 9627–9629.

Cong, L., Lu, S., Jiang, P., Zheng, T., Yu, Z., Lü, X., 2024. CO_2 sequestration and soil improvement in enhanced rock weathering: a review from an experimental perspective. Greenhouse Gases: Sci. Technol. 14 (6), 1122–1138.

Conwell, C.T., Saltzman, M.R., Edwards, C.T., Griffith, E.M., Adiatma, Y.D., 2022. Nd isotopic evidence for enhanced mafic weathering leading to Ordovician cooling. Geology 50 (8), 886–890.

Das, A., Krishnaswami, S., Sarin, M.M., Pande, K., 2005. Chemical weathering in the Krishna Basin and Western Ghats of the Deccan Traps, India: rates of basalt weathering and their controls. Geochem. Cosmochim. Acta 69 (8), 2067–2084.

Deng, H., Sonnenthal, E., Arora, B., Breunig, H., Brodie, E., Kleber, M., Spycher, N., Nico, P., 2023. The environmental controls on efficiency of enhanced rock weathering in soils. Sci. Rep. 13 (1), 9765.

Dessert, C., Dupré, B., Gaillardet, J., François, L.M., Allègre, C.J., 2003. Basalt weathering laws and the impact of basalt weathering on the global carbon cycle. Chem. Geol. 202 (3–4), 257–273.

Diakoulaki, D., Mavrotas, G., Papayannakis, L., 1995. Determining objective weights in multiple criteria problems: the CRITIC method. Comput. Oper. Res. 22 (7), 763–770.

Dupla, X., Claustre, R., Bonvin, E., Graf, I., Le Bayon, R.C., Grand, S., 2024. Let the dust settle: impact of enhanced rock weathering on soil biological, physical, and geochemical fertility. Sci. Total Environ. 954, 176297.

Dupla, X., Möller, B., Baveye, P.C., Grand, S., 2023. Potential accumulation of toxic trace elements in soils during enhanced rock weathering. Eur. J. Soil Sci. 74 (1), e13343.

Etheridge, D.M., Steele, L.P., Langenfelds, R.L., Francey, R.J., Barnola, J.M., Morgan, V. I., 1996. Natural and anthropogenic changes in atmospheric CO_2 over the last 1000 years from air in Antarctic ice and firn. J. Geophys. Res. Atmos. 101 (D2), 4115–4128.

Eufrasio, R.M., Kantzas, E.P., Edwards, N.R., Holden, P.B., Pollitt, H., Mercure, J.F., Koh, S.C., Beerling, D.J., 2022. Environmental and health impacts of atmospheric CO_2 removal by enhanced rock weathering depend on nations' energy mix. Commun. Earth Environ. 3 (1), 106.

Flipkens, G., Blust, R., Town, R.M., 2021. Deriving Nickel (Ni (II)) and Chromium (Cr (III)) based environmentally safe olivine guidelines for coastal enhanced silicate weathering. Environ. Sci. Technol. 55 (18), 12362–12371.

Foteinis, S., Campbell, J., Renforth, P., 2023. Life cycle assessment of coastal enhanced weathering for carbon dioxide removal from air. Environ. Sci. Technol. 57, 6169–6178.

Fu, H., Jian, X., Pan, H., 2023. Bias in sediment chemical weathering intensity evaluation: a numerical simulation study. Earth Sci. Rev. 246, 104574.

Fuhrman, J., Bergero, C., Weber, M., Monteith, S., Wang, F.M., Clarens, A.F., Doney, S.C., Shobe, W., McJeon, H., 2023. Diverse carbon dioxide removal approaches could reduce impacts on the energy–water–land system. Nat. Clim. Change 13 (4), 341–350.

Gao, K., Xu, J., Gao, G., Li, Y., Hutchins, D.A., Huang, B., Wang, L., Zheng, Y., Jin, P., Cai, X., Häder, D., Li, W., Xu, K., Liu, N., Riebesell, U., 2012. Rising CO_2 and increased light exposure synergistically reduce marine primary productivity. Nat. Clim. Change 2 (7), 519–523.

Gard, M., Hasterok, D., Halpin, J.A., 2019. Global whole-rock geochemical database compilation. Earth Syst. Sci. Data 11 (4), 1553–1566.

Gaucher, Y., Tanaka, K., Johansson, D.J., Goll, D.S., Ciais, P., 2025. Leveraging ecosystems responses to enhanced rock weathering in mitigation scenarios. Nat. Commun. 16 (1), 3021.

Goddéris, Y., Donnadieu, Y., Carretier, S., Aretz, M., Dera, G., Macouin, M., Regard, V., 2017. Onset and ending of the late Palaeozoic ice age triggered by tectonically paced rock weathering. Nat. Geosci. 10 (5), 382–386.

Goll, D.S., Ciais, P., Amann, T., Buermann, W., Chang, J., Eker, S., Hartmann, J., Janssens, I., Li, W., Obersteiner, M., Penuelas, J., Tanaka, K., Vicca, S., 2021. Potential CO_2 removal from enhanced weathering by ecosystem responses to powdered rock. Nat. Geosci. 14 (8), 545–549.

Guo, F., Sun, H., Yang, J., Zhang, L., Mu, Y., Wang, Y., Wu, F., 2023. Improving food security and farmland carbon sequestration in China through enhanced rock weathering: field evidence and potential assessment in different humid regions. Sci. Total Environ. 903, 166118.

Guo, X., Li, H., Yu, H., Li, W., Ye, Y., Biswas, A., 2018. Drivers of spatio-temporal changes in paddy soil pH in Jiangxi Province, China from 1980 to 2010. Sci. Rep. 8 (1), 2702.

Hakim, K., Bower, D.J., Tian, M., Deitrick, R., Auclair-Desrotour, P., Kitzmann, D., Dorn, C., Mezger, K., Heng, K., 2021. Lithologic controls on silicate weathering regimes of temperate planets. Planet. Sci. J. 2 (2), 49.

Hamilton, S.K., Kurzman, A.L., Arango, C., Jin, L., Robertson, G.P., 2007. Evidence for carbon sequestration by agricultural liming. Glob. Biogeochem. Cycles 21. GB2021.

Han, Y., Yi, D., Ye, Y., Guo, X., Liu, S., 2022. Response of spatiotemporal variability in soil pH and associated influencing factors to land use change in a red soil hilly region in southern China. Catena 212, 106074.

Haque, F., Chiang, Y.W., Santos, R.M., 2020. Risk assessment of Ni, Cr, and Si release from alkaline minerals during enhanced weathering. Open Agricul. 5 (1), 166–175.

Hartmann, J., West, A.J., Renforth, P., Köhler, P., De La Rocha, C.L., Wolf-Gladrow, D.A., Dürr, H.H., Scheffran, J., 2013. Enhanced chemical weathering as a geoengineering strategy to reduce atmospheric carbon dioxide, supply nutrients, and mitigate ocean acidification. Rev. Geophys. 51 (2), 113–149.

Hartmann, J., Moosdorf, N., 2012. The new global lithological map database GLiM: a representation of rock properties at the Earth surface. G-cubed 13 (12), Q12004.

He, J., Garzanti, E., Dinis, P., Yang, S., Wang, H., 2020. Provenance versus weathering control on sediment composition in tropical monsoonal climate (South China)—1. Geochemistry and clay mineralogy. Chem. Geol. 558, 119860.

Heřmanská, M., Voigt, M.J., Marieni, C., Declercq, J., Oelkers, E.H., 2022. A comprehensive and internally consistent mineral dissolution rate database: part I: primary silicate minerals and glasses. Chem. Geol. 597, 120807.

Hill, R.D., Peart, M.R., 1998. Land use, runoff, erosion and their control: a review for southern China. Hydrol. Process. 12 (13–14), 2029–2041.

Holden, F., Davies, K., Bird, M., Hume, R., Green, H., Beerling, D., Nelson, P., 2024. In-field carbon dioxide removal via weathering of crushed basalt applied to acidic tropical agricultural soil. Sci. Total Environ. 995, 176568.

Holzer, I.O., Nocco, M.A., Houlton, B.Z., 2023. Direct evidence for atmospheric carbon dioxide removal via enhanced weathering in cropland soil. Environ. Res. Commun. 5 (10), 101004.

Horowitz, C.A., 2016. Paris agreement. Int. Leg. Mater. 55 (4), 740–755.

Huang, S.W., Lee, Y.T., Chen, J.C., Ho, K.S., Lin, M.L., Hu, Y.T., Huang, R.Y., 2013a. Geochemistry of ultramafic xenoliths in Cenozoic alkali basalts from Jiangsu province, eastern China and their geological implication. J. Earth Syst. Sci. 122 (3), 777–793.
Huang, X.L., Niu, Y., Xu, Y.G., Ma, J.L., Qiu, H.N., Zhong, J.W., 2013b. Geochronology and geochemistry of Cenozoic basalts from eastern Guangdong, SE China: constraints on the lithosphere evolution beneath the northern margin of the South China Sea. Contrib. Mineral. Petrol. 165, 437–455.
Huang, Y., Sun, W., Qin, Z., Zhang, W., Yu, Y., Li, T., Zhang, P., 2022. The role of China's terrestrial carbon sequestration 2010–2060 in offsetting energy-related CO_2 emissions. Natl. Sci. Rev. 9 (8) nwac057.
Intergovernmental Panel on Climate Change (IPCC), 2021. Climate Change 2021: the Physical Science Basis. Contribution of Working Group I to the Sixth Assessment Report of the Intergovernmental Panel on Climate Change. Cambridge University Press.
Jamshaid, H., Mishra, R., 2016. A green material from rock: Basalt fiber–a review. J. Text. Inst. 107 (7), 923–937.
John, D.A., Leventhal, J.S., 1995. Bioavailability of metals. Geologic Aspects of Trace Elements in the Environment. USGS Publications Warehouse, pp. 37–56.
Johnson, C.C., Breward, N., Ander, E.L., Ault, L., 2005. G-BASE: baseline geochemical mapping of Great Britain and Northern Ireland. Geochem. Explor. Environ. Anal. 5 (4), 347–357.
Kantola, I.B., Blanc-Betes, E., Masters, M.D., Chang, E., Marklein, A., Moore, C.E., Haden, A.V., Bernacchi, C.J., Wolf, A., Epihov, D.Z., Beerling, D.J., DeLucia, E.H., 2023. Improved net carbon budgets in the US Midwest through direct measured impacts of enhanced weathering. Glob. Change Biol. 29 (24), 7012–7028.
Kantzas, E.P., Val Martin, M., Lomas, M.R., Eufrasio, R.M., Renforth, P., Lewis, A.L., Beerling, D.J., 2022. Substantial carbon drawdown potential from enhanced rock weathering in the United Kingdom. Nat. Geosci. 15 (5), 382–389.
Kasting, J.F., Catling, D., 2003. Evolution of a habitable planet. Annu. Rev. Astron. Astrophys. 41 (1), 429–463.
Keeling, R.F., Piper, S.C., Bollenbacher, A.F., Walker, S.J., 2001. Atmospheric CO_2 concentrations from the NOAA/CMDL Carbon Cycle Greenhouse Gases Group (No. NDPSC/DATA001). Carbon Dioxide Information Analysis Center. Oak Ridge National Laboratory.
Kelland, M.E., Wade, P.W., Lewis, A.L., Taylor, L.L., Sarkar, B., Andrews, M.G., Lomas, M.R., Cotton, T.E.A., Kemp, S.J., James, R.H., Pearce, C.R., Hartley, S.E., Hodson, M.E., Leake, J.R., Banwart, S.A., Beerling, D.J., 2020. Increased yield and CO2 sequestration potential with the C4 cereal Sorghum bicolor cultivated in basaltic rock dust-amended agricultural soil. Glob. Change Biol. 26 (6), 3658–3676.
Khalidy, R., Chiang, Y.W., Santos, R.M., 2023. Fate and migration of enhanced rock weathering products through soil horizons; implications of irrigation and percolation regimes. Catena 233, 107524.
Köhler, P., Hartmann, J., Wolf-Gladrow, D.A., 2010. Geoengineering potential of artificially enhanced silicate weathering of olivine. Proc. Natl. Acad. Sci. 107 (47), 20228–20233.
Kierczak, J., Pietranik, A., Pędziwiatr, A., 2021. Ultramafic geoecosystems as a natural source of Ni, Cr, and Co to the environment: a review. Sci. Total Environ. 755, 142620.
Lan, X., Tans, P., Thoning, K.W., 2025. Trends in globally-averaged CO_2 Determined from NOAA Global Monitoring Laboratory Measurements (Version 2025-05). NOAA Global Monitoring Laboratory.
Larkin, C.S., Andrews, M.G., Pearce, C.R., Yeong, K.L., Beerling, D.J., Bellamy, J., James, R.H., 2022. Quantification of CO_2 removal in a large-scale enhanced weathering field trial on an oil palm plantation in Sabah, Malaysia. Front. Clim. 4, 959229.
Lee, C.-T.A., Jiang, H., Dasgupta, R., Torres, M., 2019. A framework for understanding whole-earth carbon cycling. In: Orcutt, B.N., Daniel, I., Dasgupta, R. (Eds.), Deep Carbon: past to Present. Cambridge University Press, Cambridge, pp. 313–357 chapter.
Lee, R.J., Strohmeier, B.R., Bunker, K.L., Van Orden, D.R., 2008. Naturally occurring asbestos—A recurring public policy challenge. J. Hazard Mater. 153 (1-2), 1–21.
Levy, C.R., Almaraz, M., Beerling, D.J., Raymond, P., Reinhard, C.T., Suhrhoff, T.J., Taylor, L., 2024. Enhanced rock weathering for carbon removal-monitoring and mitigating potential environmental impacts on agricultural land. Environ. Sci. Technol. 58 (39), 17215–17226.
Li, B., Jiang, S.Y., Zhang, Q., Zhao, H.X., Zhao, K.D., 2015. Cretaceous crust-mantle interaction and tectonic evolution of Cathaysia Block in South China: evidence from pulsed mafic rocks and related magmatism. Tectonophysics 661, 136–155.
Li, J., Zhang, Y., Dong, S., Johnston, S.T., 2014. Cretaceous tectonic evolution of South China: a preliminary synthesis. Earth Sci. Rev. 134, 98–136.
Li, Y.Q., Kitagawa, H., Nakamura, E., Ma, C., Hu, X., Kobayashi, K., Sakaguchi, C., 2020. Various ages of recycled material in the source of Cenozoic basalts in Southeast China: implications for the role of the Hainan Plume. J. Petrol. 61 (6) egaa060.
Linke, T., Oelkers, E., Möckel, S., Gislason, S., 2024. Direct evidence of CO2 drawdown through enhanced weathering in soils. Goldschmidt.
Luan, Y., Song, X.Y., Chen, L.M., Zheng, W.Q., Zhang, X.Q., Yu, S.Y., Ran, Q.Y., 2014. Key factors controlling the accumulation of the Fe-Ti oxides in the Hongge layered intrusion in the Emeishan Large Igneous Province, SW China. Ore Geol. Rev. 57, 518–538.
Manning, D.A., Renforth, P., Lopez-Capel, E., Robertson, S., Ghazireh, N., 2013. Carbonate precipitation in artificial soils produced from basaltic quarry fines and composts: an opportunity for passive carbon sequestration. Int. J. Greenh. Gas Control 17, 309–317.
Marzini, L., Iannini, M., Giorgetti, G., Bonciani, F., Conti, P., Salvini, R., Viti, C., 2024. Asbestos hazard in serpentinite rocks: influence of mineralogical and structural characteristics on fiber potential release. Geosciences 14 (8), 210.
Matter, J.M., Stute, M., Snæbjörnsdottir, S.Ó., Oelkers, E.H., Gislason, S.R., Aradottir, E. S., Sigfusson, B., Gunnarsson, I., Sigurdardottir, H., Gunnlaugsson, E., Axelsson, G., Alfredsson, H.A., Wolff-Boenisch, D., Mesfin, K., Taya, D.F.D.L.R., Hall, J., Dideriksen, K., Broecker, W.S., 2016. Rapid carbon mineralization for permanent disposal of anthropogenic carbon dioxide emissions. Science 352 (6291), 1312–1314.
McGrail, B.P., Schaef, H.T., Spane, F.A., Cliff, J.B., Qafoku, O., Horner, J.A., Thompson, C.J., Owen, A.T., Sullivan, C.E., 2017. Field validation of supercritical CO_2 reactivity with basalts. Environ. Sci. Technol. Lett. 4 (1), 6–10.
McLennan, S.M., 1993. Weathering and global denudation. J. Geol. 101 (2), 295–303.
Meysman, F.J., Montserrat, F., 2017. Negative CO_2 emissions via enhanced silicate weathering in coastal environments. Biol. Lett. 13 (4), 20160905.
Monnin, E., Indermühle, A., Dällenbach, A., Flückiger, J., Stauffer, B., Stocker, T.F., Raynaud, D., Barnola, J., 2001. Atmospheric CO_2 concentrations over the last glacial termination. Science 291 (5501), 112–114.
Moosdorf, N., Renforth, P., Hartmann, J., 2014. Carbon dioxide efficiency of terrestrial enhanced weathering. Environ. Sci. Technol. 48 (9), 4809–4816.
Murray, J., Jagoutz, O., 2024. Palaeozoic cooling modulated by ophiolite weathering through organic carbon preservation. Nat. Geosci. 17 (1), 88–93.
Odu, G.O., 2019. Weighting methods for multi-criteria decision making technique. J. Appl. Sci. Environ. Manag. 23 (8), 1449–1457.
Penman, D.E., Rugenstein, J.K.C., Ibarra, D.E., Winnick, M.J., 2020. Silicate weathering as a feedback and forcing in Earth's climate and carbon cycle. Earth Sci. Rev. 209, 103298.
Ramos, C.G., Hower, J.C., Blanco, E., Oliveira, M.L.S., Theodoro, S.H., 2022. Possibilities of using silicate rock powder: an overview. Geosci. Front. 13 (1), 101185.
Ren, S.L., Li, J.L., Zhou, X.H., Sun, M., 1997. Petrochemistry and mineral chemistry studies on metamorphic ultramafic rocks in Yanghou area, Zhenghe Country, Fujian Province, China. Geochimica 26 (4), 13–23.
Renforth, P., 2012. The potential of enhanced weathering in the UK. Int. J. Greenh. Gas Control 10, 229–243.
Renforth, P., von Strandmann, P.P., Henderson, G.M., 2015. The dissolution of olivine added to soil: implications for enhanced weathering. Appl. Geochem. 61, 109–118.
Renforth, P., Henderson, G., 2017. Assessing ocean alkalinity for carbon sequestration. Rev. Geophys. 55, 636–674.
Riebesell, U., Schulz, K.G., Bellerby, R.G.J., Botros, M., Fritsche, P., Meyerhöfer, M., Neill, C., Nondal, G., Oschlies, A., Wohlers, J., Zöllner, E., 2007. Enhanced biological carbon consumption in a high CO_2 ocean. Nature 450 (7169), 545–548.
Rinder, T., von Hagke, C., 2021. The influence of particle size on the potential of enhanced basalt weathering for carbon dioxide removal: insights from a regional assessment. J. Clean. Prod. 315, 128178.
Schott, J., Pokrovsky, O.S., Spalla, O., Devreux, F., Gloter, A., Mielczarski, J.A., 2012. Formation, growth and transformation of leached layers during silicate minerals dissolution: the example of wollastonite. Geochem. Cosmochim. Acta 98, 259–281.
Schuiling, R.D., Krijgsman, P., 2006. Enhanced weathering: an effective and cheap tool to sequester CO_2. Clim. Change 74 (1), 349–354.
Shakun, J.D., Clark, P.U., He, F., Marcott, S.A., Mix, A.C., Liu, Z., Otto-Bliesner, B., Schmittner, A., Bard, E., 2012. Global warming preceded by increasing carbon dioxide concentrations during the last deglaciation. Nature 484 (7392), 49–54.
Shellnutt, J.G., 2014. The Emeishan large igneous province: a synthesis. Geosci. Front. 5 (3), 369–394.
Shepard, D., 1968. A two-dimensional interpolation function for irregularly-spaced data. Proceedings of the 1968 ACM National Conference, pp. 517–524.
Shu, Liangshu, Yao, Jinlong, Wang, Bo, Faure, Michel, Charvet, Jacques, et al., 2021. Neoproterozoic plate tectonic process and Phanerozoic geodynamic evolution of the South China Block. Earth-Science Reviews 216, 103596. https://doi.org/10.1016/j.earscirev.2021.103596, 103596. https://linkinghub.elsevier.com/retrieve/pii/S0012825221000969.
Skov, K., Wardman, J., Healey, M., McBride, A., Bierowiec, T., Cooper, J., Liu, X., 2024. Initial agronomic benefits of enhanced weathering using basalt: a study of spring oat in a temperate climate. PLoS One 19 (3), e0295031.
Smith, S.M., Geden, O., Gidden, M.J., Lamb, W.F., Nemet, G.F., Minx, J.C., Buck, H., Burke, J., Cox, E., Edwards, M.R., Fuss, S., Johnstone, I., Müller-Hansen, F., Pongratz, J., Probst, B.S., Roe, S., Schenuit, F., Schulte, I., Vaughan, N.E., 2024. The State of Carbon Dioxide Removal. The State of Carbon Dioxide Removal, second ed.
Sokol, N.W., Sohng, J., Moreland, K., Slessarev, E., Goertzen, H., Schmidt, R., Scow, K., 2024. Reduced accrual of mineral-associated organic matter after two years of enhanced rock weathering in cropland soils, though no net losses of soil organic carbon. Biogeochemistry 167 (8), 989–1005.
Spence, E., Cox, E., Pidgeon, N., 2021. Exploring cross-national public support for the use of enhanced weathering as a land-based carbon dioxide removal strategy. Clim. Change 165 (1), 23.
Strefler, J., Amann, T., Bauer, N., Kriegler, E., Hartmann, J., 2018. Potential and costs of carbon dioxide removal by enhanced weathering of rocks. Environ. Res. Lett. 13 (3), 034010.
Su, C., Kang, R., Huang, W., Wang, A., Li, X., Huang, K., Zhou, Q., Fang, Y., 2025. CO_2 removal with enhanced wollastonite weathering in acidic and calcareous soils. Soil Ecol. Lett. 7 (1), 1–11.
Sun, Y., Guo, G., Shi, H., Liu, M., Keith, A., Li, H., Jones, K.C., 2020. Decadal shifts in soil pH and organic matter differ between land uses in contrasting regions in China. Sci. Total Environ. 740, 139904.
Sun, Y., Yang, J., Li, K., Gong, J., Gao, J., Wang, Z., Cai, Y., Zhao, K., Hu, S., Fu, Y., Duan, Z., Lin, L., 2023. Differentiating environmental scenarios to establish

geochemical baseline values for heavy metals in soil: a case study of Hainan Island, China. Sci. Total Environ. 898, 165634.
Taylor, L.L., Quirk, J., Thorley, R.M., Kharecha, P.A., Hansen, J., Ridgwell, A., Lomas, M. R., Banwart, S.A., Beerling, D.J., 2016. Enhanced weathering strategies for stabilizing climate and averting ocean acidification. Nat. Clim. Change 6 (4), 402–406.
te Pas, E.E., Hagens, M., Comans, R.N., 2023. Assessment of the enhanced weathering potential of different silicate minerals to improve soil quality and sequester CO_2. Front. Clim. 4, 954064.
Terlouw, T., Bauer, C., Rosa, L., Mazzotti, M., 2021. Life cycle assessment of carbon dioxide removal technologies: a critical review. Energy Environ. Sci. 14 (4), 1701–1721.
United Nations Framework Convention on Climate Change, 2015. Adoption of the Paris agreement. FCCC/CP/2015/L.9/Rev.1).
Van Der Bauwhede, R., Muys, B., Vancampenhout, K., Smolders, E., 2024. Accelerated weathering of silicate rock dusts predicts the slow-release liming in soils depending on rock mineralogy, soil acidity, and test methodology. Geoderma 441, 116734.
Van Groenigen, K.J., Osenberg, C.W., Hungate, B.A., 2011. Increased soil emissions of potent greenhouse gases under increased atmospheric CO_2. Nature 475 (7355), 214–216.
Vanderkloot, E., Ryan, P., 2023. Quantifying the effect of grain size on weathering of basaltic powders: implications for negative emission technologies via soil carbon sequestration. Appl. Geochem. 155, 105728.
Vienne, A., Poblador, S., Portillo-Estrada, M., Hartmann, J., Ijiehon, S., Wade, P., Vicca, S., 2022. Enhanced weathering using basalt rock powder: carbon sequestration, co-benefits and risks in a mesocosm study with Solanum tuberosum. Front. Clim. 4, 869456.
Wu, W., Qu, S., Nel, W., Ji, J., 2021. The influence of natural weathering on the behavior of heavy metals in small basaltic watersheds: a comparative study from different regions in China. Chemosphere 262, 127897.
Xiong, R., He, X., Gao, N., Li, Q., Qiu, Z., Hou, Y., Shen, W., 2024. Soil pH amendment alters the abundance, diversity, and composition of microbial communities in two contrasting agricultural soils. Microbiol. Spectr. 12 (8), e04165, 23.
Xu, T., Li, H., Vicca, S., Goll, D.S., Beerling, D.J., Chen, Q., Bi, B., Yang, Z., Wang, X., Yuan, Z., 2025. Enhanced rock weathering promotes soil organic carbon accumulation: a global meta-analysis based on experimental evidence. Glob. Change Biol. 31 (9), e70483.
Xu, T., Yuan, Z., Vicca, S., Goll, D.S., Li, G., Lin, L., Chen, H., Bi, B., Chen, Q., Li, C., Wang, X., Wang, C., Hao, Z., Fang, Y., Beerling, D.J., 2024. Enhanced silicate weathering accelerates forest carbon sequestration by stimulating the soil mineral carbon pump. Glob. Change Biol. 30 (8), e17464.
Xu, Y., Chung, S.L., Jahn, B.M., Wu, G., 2001. Petrologic and geochemical constraints on the petrogenesis of Permian–Triassic Emeishan flood basalts in southwestern China. Lithos 58 (3–4), 145–168.
Xue, D., Lu, J., Leung, L.R., Teng, H., Song, F., Zhou, T., Zhang, Y., 2023. Robust projection of East Asian summer monsoon rainfall based on dynamical modes of variability. Nat. Commun. 14 (1), 3856.
Yan, Y., Dong, X., Li, R., Zhang, Y., Yan, S., Guan, X., Yang, Q., Chen, L., Fang, Y., Zhang, W., Wang, S., 2023. Wollastonite addition stimulates soil organic carbon mineralization: evidences from 12 land-use types in subtropical China. Catena 225, 107031.
Yang, J., Wei, H., Zhang, J., Shi, Z., Li, H., Ye, Y., Abdo, A.I., 2022. Land use and soil type exert strongly interactive impacts on the pH buffering capacity of acidic soils in South China. Sustainability 14 (19), 12891.
Yang, Jie, Huang, Xin, 2024. The 30 m annual land cover datasets and its dynamics in China from 1985 to 2023. In: Earth System Science Data, vol. 13. Zenodo, pp. 3907–3925, 1.0.3No. 1.
Yao, T., Li, H.M., Li, W.J., Li, L.X., Zhao, C., 2015. Origin of the disseminated magnetite pyroxenite in the Tieshanmiao-type iron deposits in the Wuyang region of Henan Province, China. J. Asian Earth Sci. 113, 1235–1252.
You, Q., Jiang, Z., Yue, X., Guo, W., Liu, Y., Cao, J., Li, W., Wu, F., Cai, Z., Zhu, H., Li, T., Liu, Z., He, J., Chen, D., Pepin, N., Zhai, P., 2022. Recent frontiers of climate changes in East Asia at global warming of 1.5 °C and 2 °C. npj Clim. Atmos. Sci. 5 (1), 80.
Zhang, B., Kroeger, J., Planavsky, N., Yao, Y., 2023. Techno-economic and life cycle assessment of enhanced rock weathering: a case study from the Midwestern United States. Environ. Sci. Technol. 57 (37), 13828–13837.
Zhang, S., Jian, X., Liu, J.T., Wang, P., Chang, Y.P., Zhang, W., 2022. Climate-driven drainage reorganization of small mountainous rivers in Taiwan (East Asia) since the last glaciation: the Zhuoshui River example. Palaeogeogr. Palaeoclimatol. Palaeoecol. 586, 110759.
Zhou, M.F., Robinson, P.T., Lesher, C.M., Keays, R.R., Zhang, C.J., Malpas, J., 2005. Geochemistry, petrogenesis and metallogenesis of the Panzhihua gabbroic layered intrusion and associated Fe-Ti-V oxide deposits, Sichuan Province, Southwest China. J. Petrol. 46 (11), 2253–2280.
Zhou, X., Sun, T., Shen, W., Shu, L., Niu, Y., 2006. Petrogenesis of Mesozoic granitoids and volcanic rocks in South China: a response to tectonic evolution. Episodes J. Int. Geosci. 29 (1), 26–33.
Zhou, Y., Sun, S., Feng, Z., Xu, C., Cai, Y., Liang, X., Liu, X., Du, Y., 2021. A new insight into the eastern extension of the Proto-Tethyan margin of Gondwana by early Paleozoic volcanic rocks in South China. Lithos 398, 106328.